Actin-dependent recruitment of AGO2 to the zonula adherens

Mary Catherine Bridges, Joyce Nair-Menon, Alyssa Risner, Douglas W. Jimenez, Amanda C. Daulagala, Christina Kingsley, Madison E. Davis, and Antonis Kourtidis*
Department of Regenerative Medicine and Cell Biology, Medical University of South Carolina, 173 Ashley Avenue, Charleston, SC 29425

ABSTRACT **Adherens junctions are cadherin-based structures critical for cellular architecture. E-cadherin junctions in mature epithelial cell monolayers tether to an apical actomyosin ring to form the zonula adherens (ZA). We have previously shown that the adherens junction protein PLEKHA7 associates with and regulates the function of the core RNA interference (RNAi) component AGO2 specifically at the ZA. However, the mechanism mediating AGO2 recruitment to the ZA remained unexplored. Here, we reveal that this ZA-specific recruitment of AGO2 depends on both the structural and tensile integrity of the actomyosin cytoskeleton. We found that depletion of not only PLEKHA7, but also either of the three PLEKHA7-interacting, LIM-domain family proteins, namely LMO7, LIMCH1, and PDLIM1, results in disruption of actomyosin organization and tension, as well as disruption of AGO2 junctional localization and of its miRNA-binding ability. We also show that AGO2 binds Myosin IIB and that PLEKHA7, LMO7, LIMCH1, and PDLIM1 all disrupt interaction of AGO2 with Myosin IIB at the ZA. These results demonstrate that recruitment of AGO2 to the ZA is sensitive to actomyosin perturbations, introducing the concept of mechanosensitive RNAi machinery, with potential implications in tissue remodeling and in disease.**

SIGNIFICANCE STATEMENT

- Previous work has shown that PLEKHA7 recruits core RNAi components, including AGO2, to regulate tumor-suppressing miRNAs specifically at the zonula adherens (ZA), through an unknown mechanism.
- Here, the authors show that three LIM domain-containing proteins, LMO7, LIMCH1, and PDLIM1, are also responsible for AGO2's recruitment and miRNA activity at the ZA and that all four PLEKHA7, LMO7, LIMCH1, and PDLIM1 mediate AGO2 recruitment to the ZA not due to their protein–protein interactions, but through stabilizing actomyosin structure and tension.
- These findings introduce a mechanosensitive RNAi machinery responsive to actomyosin perturbations, with potentially broad implications in regulation of cellular plasticity.

Monitoring Editor
Alpha Yap
University of Queensland

Received: Mar 17, 2022
Revised: Sep 18, 2023
Accepted: Oct 4, 2023

This article was published online ahead of print in MBoC in Press (http://www.molbiolcell.org/cgi/doi/10.1091/mbc.E22-03-0099-T) on October 11, 2023.

*Address correspondence to: Antonis Kourtidis (kourtidi@musc.edu).

Abbreviations used: ACTN1, actinin alpha 1; AGO2, Argonaute 2; AJ, adherens junction; ANOVA, analysis of variance; ATCC, American Type Culture Collection; BCA, bicinchoninic acid; Blebb, Blebbistatin; cDNA, complementary DNA; CGNL1, cingulin like 1; cm, centimeter; CRISPR, clustered regularly interspaced short palindromic repeats; DAPI, 4-,6-diamidino-2-phenylindole; DIC, differential interference contrast; DMEM, Dulbecco's Modified Eagle Medium; DMSO, dimethylsulfoxide; DTT, dithiothreitol; Ecad, E-cadherin; ECM, extracellular matrix; EDTA, ethylenediaminetetraacetic acid; EGTA, ethylene glycol-bis(β-aminoethyl ether)-*N*,*N*,*N*′,*N*′-tetraacetic acid; FBS, fetal bovine serum; FDR, false discovery rate; GO, Gene Ontology; h, hours; HEK 293FT, human embryonic kidney 293FT cells; HEPES, 4-(2-hydroxyethyl)-1-piperazineethanesulfonic acid; HRP, horseradish peroxidase; IB, immunoblot; IgG, immunoglobulin G; IP, immunoprecipitation; kD, kilodalton; KO, knockout; LatA, Latrunculin A; LIMCH1, LIM and calponin homology domains 1; LIMD1, LIM domain containing 1; LMO7, LIM domain 7; MDCK, Madin-Darby canine kidney cells; MEM, minimum essential medium; min, minutes; miRNA, microRNA; mM, millimolar; MRLC, myosin II regulatory light chain; mRNA, messenger RNA; Ms, mouse; NaCl, sodium chloride; NEAA, non-essential amino acids; NT, non-target; O/N, overnight; p-body, processing body; p120, p120 catenin; PBS, phosphate-buffered saline; PDLIM1, PDZ and LIM domain 1; PLA, proximity ligation assay; PLEKHA7, Pleckstrin homology domain containing A7; qRT-PCR, quantitative reverse transcription polymerase chain reaction; Rb, rabbit; RIPA, radioimmunoprecipitation assay; RISC, RNA-induced silencing complex; RITS-like, RNA-induced transcriptional gene silencing–like; RNAi, RNA interference; ROCK, Rho associated coiled-coil containing protein kinase; RT, room temperature; SD, standard deviation; SDS-PAGE, sodium dodecyl sulfate polyacrylamide gel electrophoresis; SDS, sodium dodecyl sulfate; sgRNA, single guide RNA; shRNA, short hairpin RNA; U/ml, units/milliliter; WT, wild type; WTIP, wilms tumor protein 1-interacting protein; ZA, zonula adherens; µg, microgram; µl, microliter; µm, micrometer; µM, micromolar.

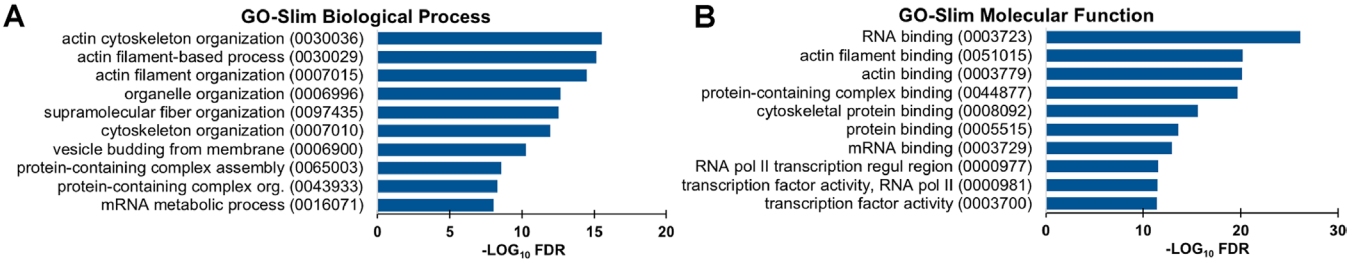

C

Gene ID	Gene name	Unique peptides
LMO7	LIM domain only protein 7	53
LIMCH1	LIM and calponin homology domains-containing protein 1	17
PDLIM1	PDZ and LIM domain protein 1	14
LIMA	LIM domain and actin-binding protein 1	6
LASP	LIM and SH3 domain protein 1	5

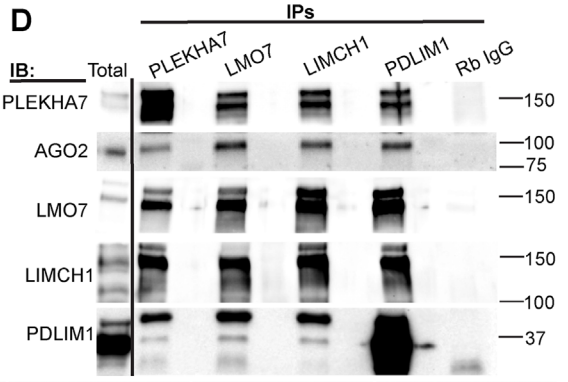

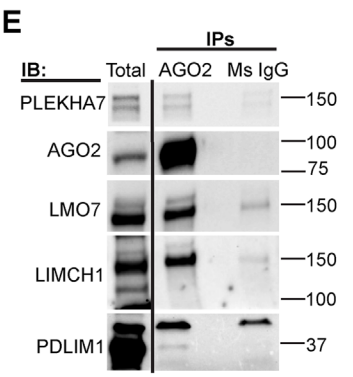

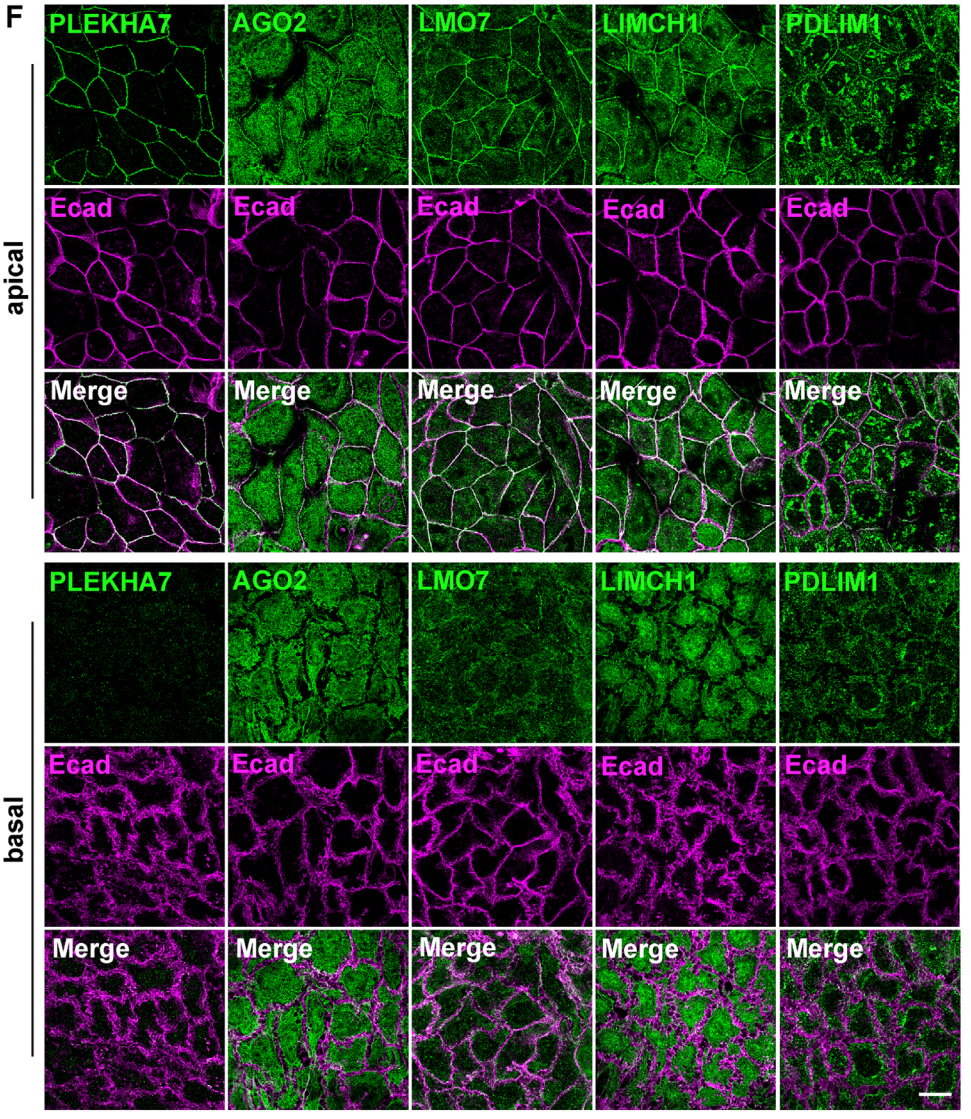

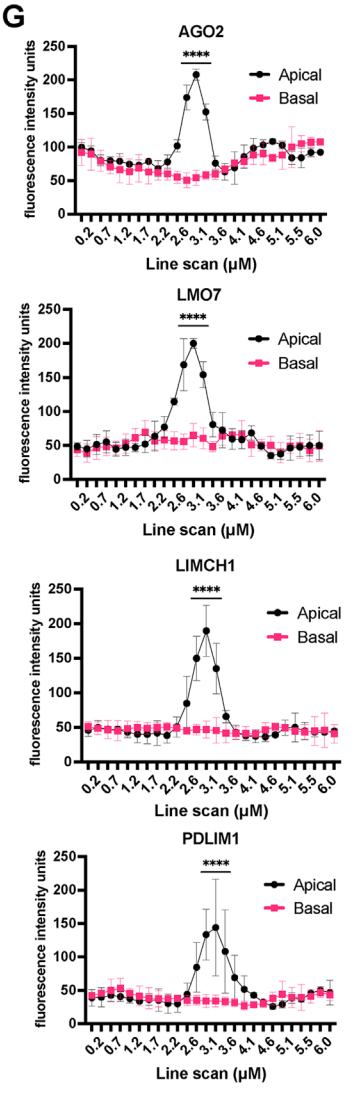

INTRODUCTION

The Adherens Junction (AJ) is a cell–cell adhesive structure essential for epithelial tissue organization and homeostasis (Meng and Takeichi, 2009; Harris and Tepass, 2010; Takeichi, 2014). E-cadherin (Ecad) is the core AJ component that forms extracellular linkages between neighboring cells through calcium-dependent homotypic binding (Takeichi, 1995). Intracellularly, Ecad binds to β-catenin and p120 catenin (p120; Reynolds *et al.*, 1994), with p120 playing a key role in stabilizing cadherin junctions (Thoreson *et al.*, 2000). Ecad-based junctions also connect to the actin cytoskeleton through α-catenin (Mege and Ishiyama, 2017), a β-catenin binding partner. In polarized epithelia, these connections mature at an apically localized structure known as the zonula adherens (ZA), which links to a circumferential actin ring (Farquhar and Palade, 1963; Meng and Takeichi, 2009). At the ZA, actin organization is intimately involved in the dynamic interplay between contractile force sensation and junctional stabilization (Kovacs *et al.*, 2002; Shewan *et al.*, 2005; Yamada and Nelson, 2007; Smutny *et al.*, 2010; Kovacs *et al.*, 2011; Ratheesh and Yap, 2012; Verma *et al.*, 2012; Priya *et al.*, 2013; Leerberg *et al.*, 2014).

In addition to their critical architectural role, epithelial AJs mediate numerous signaling pathways directing cell behavior (Kourtidis *et al.*, 2013, 2017a; Yu and Elble, 2016; Mendonsa *et al.*, 2018; Salvi and DeMali, 2018; Yulis *et al.*, 2018; Daulagala *et al.*, 2019; Ramirez Moreno and Bulgakova, 2021). This aspect of AJ biology implicates loss of AJ integrity to the progression of multiple diseases, such as cancer (Kourtidis *et al.*, 2013, 2017a; Yu and Elble, 2016; Mendonsa *et al.*, 2018; Daulagala *et al.*, 2019; Ramirez Moreno and Bulgakova, 2021). Along these lines, we have previously demonstrated that cadherin junctions recruit core complexes of the RNA interference (RNAi) machinery, such as the microprocessor, the DICER complex, and the RNA-induced Silencing Complex (RISC), to locally regulate microRNA (miRNA) processing and function (Kourtidis *et al.*, 2015, 2017b). Loading of miRNAs onto Argonaute 2 (AGO2), the main enzymatic component of the RISC, leads to translational repression or degradation of target mRNAs (Hammond *et al.*, 2001; Liu *et al.*, 2004; Meister *et al.*, 2004; Huntzinger and Izaurralde, 2011). While AGO2 has been shown to be primarily cytoplasmic, its recruitment to distinct subcellular loci is a mechanism by which RISC activity can be regulated (Leung *et al.*, 2006; Zeng *et al.*, 2008; James *et al.*, 2010; Detzer *et al.*, 2011; Antoniou *et al.*, 2014; Gagnon *et al.*, 2014; Bridge *et al.*, 2017; Bose *et al.*, 2020). Our previous work identified recruitment of AGO2 specifically to the ZA of well-differentiated epithelial cells and tissues, but not at basolateral areas of cell–cell contact (Kourtidis *et al.*, 2017b; Nair-Menon *et al.*, 2020). This recruitment was mediated by PLEKHA7 (Kourtidis *et al.*, 2015, 2017b; Nair-Menon *et al.*, 2020), a ZA-specific p120-binding partner (Meng *et al.*, 2008; Pulimeno *et al.*, 2010). We have shown that loss of junctional AGO2 localization negatively impacts AGO2-loading of a specific set of miRNAs and several of their target oncogenic mRNAs, consequently releasing RISC-mediated oncogene suppression (Kourtidis *et al.*, 2015, 2017b). Furthermore, we demonstrated that junctional localization of AGO2 is broadly lost in human colon tumors and in poorly differentiated colon cancer cell lines, even when cadherin junctions were still present, although not mature, implying for the existence of a mechanism fine-tuning recruitment of AGO2 to mature ZA of well-differentiated epithelia (Nair-Menon *et al.*, 2020).

Indeed, while PLEKHA7 is required for junctional localization of AGO2, what determines AGO2's specific recruitment to the ZA remained unclear. PLEKHA7 was originally characterized for its role in tethering the minus ends of the microtubules to the ZA (Meng *et al.*, 2008). Notably, a significant body of work demonstrates that intracellular localization of RNA-binding complexes is mediated by the microtubule cytoskeleton (Kanai *et al.*, 2004; Liao *et al.*, 2019; Denes *et al.*, 2021; Pichon *et al.*, 2021; Scarborough *et al.*, 2021). These observations led us to originally hypothesize that AGO2 recruitment to the ZA could be microtubule-directed. Surprisingly, our previous experimentation showed that AGO2, or even PLEKHA7 localization at the ZA is microtubule-independent (Kourtidis *et al.*, 2017b), leaving the mechanism of AGO2 recruitment to the ZA an open question. To obtain clues about this mechanism, we re-examined in this study our published PLEKHA7 proteome. This re-examination led us to identify three LIM domain-containing proteins as also being responsible for the recruitment of AGO2 to the ZA, in addition to PLEKHA7, and to discover that all four proteins mediate this junctional recruitment of AGO2 through stabilizing the actomyosin cytoskeleton at the ZA.

RESULTS

PLEKHA7 and AGO2 associate with LIM domain-containing proteins at the ZA

To obtain insight on the potential mechanisms involved in AGO2 recruitment to the ZA, we re-examined our published dataset of PLEKHA7-interacting proteins (publicly available at www.imexconsortium.org/; identifier: IM-25739; Kourtidis *et al.*, 2017b). In that experiment, PLEKHA7 immunoprecipitation from Caco2 well-differentiated intestinal epithelial cells and subsequent mass-spectrometry analysis identified more than 600 potential PLEKHA7 interactors (Kourtidis *et al.*, 2017b). We have reported that a significant set of these interactors are RNA-binding proteins, such as RISC components (Kourtidis *et al.*, 2017b). Here, we performed gene ontology (GO) enrichment analysis on this dataset. This analysis revealed that in addition to RNA-binding proteins, the set of PLEKHA7-associated proteins is significantly enriched for processes and functions related to the actin cytoskeleton (Figure 1, A and B). This result aligns with

FIGURE 1: PLEKHA7 interacts with AGO2 and actin-related, LIM domain-containing proteins at apical AJs. (A and B) GO enrichment analyses of the PLEKHA7-interacting protein dataset (www.imexconsortium.org/; identifier: IM-25739). The GO-slim Molecular Function and GO-slim Biological Process datasets were interrogated using Fisher's exact test with FDR correction to assess enrichment significance. The 10 most significantly enriched GO terms are shown; GO term accession numbers are displayed in parentheses. (C) LIM domain-containing proteins identified in the same dataset of PLEKHA7 interactors; the unique peptide counts recorded from mass spectrometry analysis following PLEKHA7 immunoprecipitation are shown. (D and E) Immunoprecipitation (IP) of PLEKHA7, LMO7, LIMCH1, PDLIM1, and AGO2 from Caco2 cells, immunoblotted (IB) for the same markers; IgG is the negative control. Molecular masses (kD) are indicated on the right. (F–G) Immunofluorescence of Ecad, PLEKHA7, LMO7, LIMCH1, PDLIM1, and AGO2 in confluent Caco2 cell monolayers. Images were obtained by confocal microscopy, and Z-series stacks were acquired through the entire plane; representative apical and basal Z-slices are shown. Fluorescence intensity of 6-μm line scans drawn perpendicular to cell–cell junctions was measured from $n = 30$ cell–cell junctions (10 junctions/field) representative of three independent experiments; statistical analyses were performed using two-way ANOVA tests; error bars represent mean ± SD; ****$P < 0.0001$. Scale bar = 20 μm.

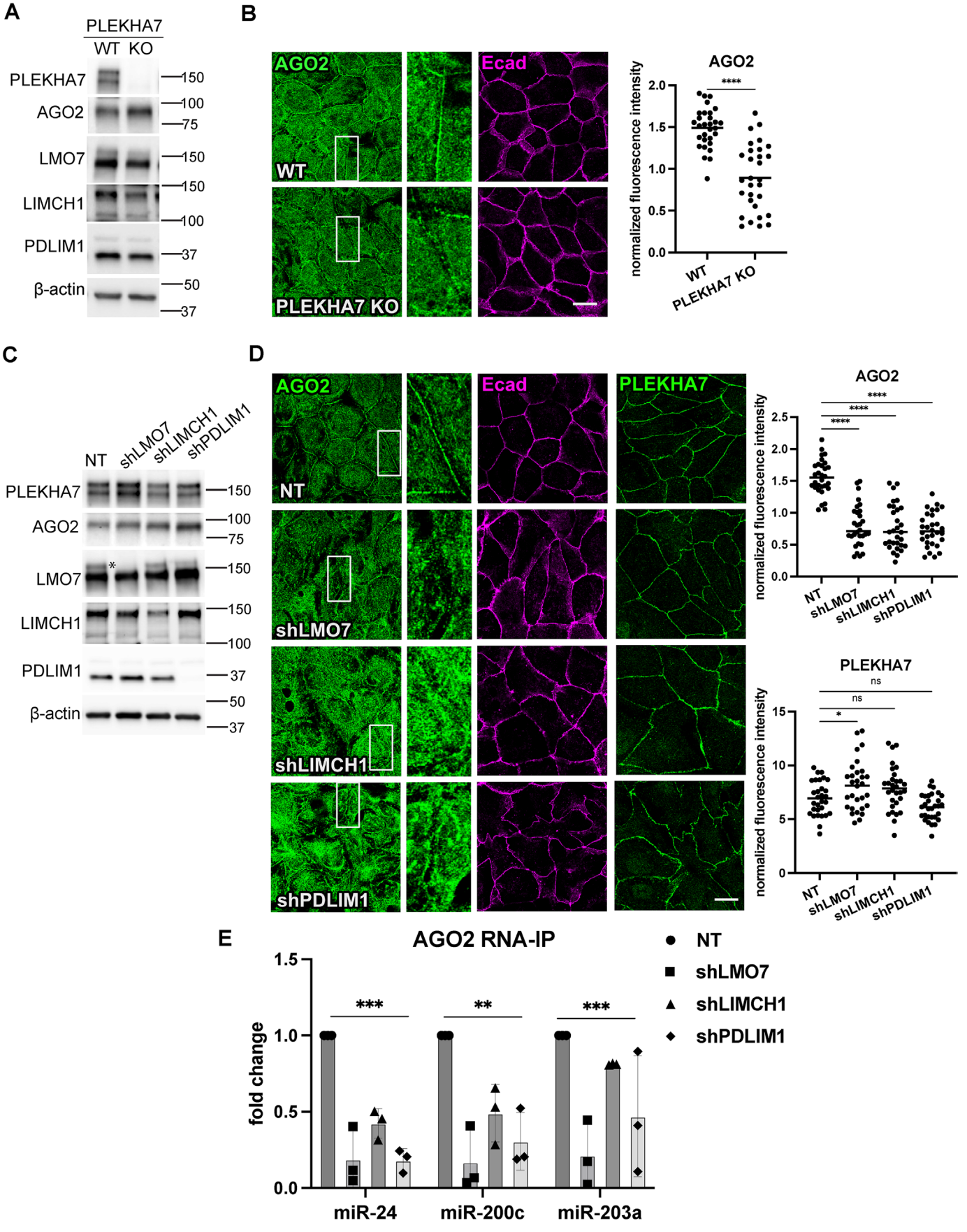
A
PLEKHA7
WT KO
PLEKHA7
AGO2
LMO7
LIMCH1
PDLIM1
β-actin
150
100
75
150
150
100
37
50
37
B
AGO2
Ecad
WT
PLEKHA7 KO
AGO2
normalized fluorescence intensity
****
WT
PLEKHA7 KO
C
NT
shLMO7
shLIMCH1
shPDLIM1
PLEKHA7
AGO2
LMO7
LIMCH1
PDLIM1
β-actin
*
150
100
75
150
150
100
37
50
37
D
AGO2
Ecad
PLEKHA7
NT
shLMO7
shLIMCH1
shPDLIM1
AGO2
normalized fluorescence intensity
****
****
****
NT
shLMO7
shLIMCH1
shPDLIM1
PLEKHA7
normalized fluorescence intensity
ns
ns
*
NT
shLMO7
shLIMCH1
shPDLIM1
E
AGO2 RNA-IP
fold change
***
**
***
miR-24
miR-200c
miR-203a
NT
shLMO7
shLIMCH1
shPDLIM1

our previous findings that PLEKHA7 stabilizes apical actin and that it associates with certain actin-binding proteins (Kourtidis *et al.*, 2015; Kourtidis and Anastasiadis, 2016). Overall, the GO analyses point to RNA-binding and actin cytoskeletal-mediated functions as the top roles in which PLEKHA7 is potentially involved.

Through examining the group of actin-related PLEKHA7 interactors, we noted several proteins belonging to the LIM domain-containing protein family (Figure 1C). These proteins attracted our attention, because LIM protein family members, such as Ajuba, LIMD1, and WTIP, have been previously implicated in AGO2 recruitment and RISC assembly in cytoplasmic p-bodies (James *et al.*, 2010; Bridge *et al.*, 2017; Tilley *et al.*, 2020). Our PLEKHA7 proteomics analysis identified a different set of proteins belonging to this same family (Figure 1C). More specifically, the LIM domain protein with the highest count of PLEKHA7-enriched unique peptides was LIM domain only protein 7 (LMO7; Figure 1C). LMO7 was previously identified to localize to apical AJs, where it plays an actin-mediated role in linking and stabilizing nectin and cadherin junctional complexes (Ooshio *et al.*, 2004). The other top enriched LIM domain-containing proteins were LIM and calponin homology domains-containing protein 1 (LIMCH1) and PDZ and LIM domain protein 1 (PDLIM1; Figure 1C). Considering the reported functions of LIM domain-containing proteins in actin (Kadrmas and Beckerle, 2004; Anderson *et al.*, 2021) and AGO2 regulation (James *et al.*, 2010; Bridge *et al.*, 2017; Tilley *et al.*, 2020), we sought to interrogate these three LIM proteins as intermediates of AGO2 recruitment to the ZA. Protein co-immunoprecipitation, followed by Western blot analysis, confirmed PLEKHA7–LMO7–LIMCH1–PDLIM1 protein interactions with each other and with AGO2 (Figure 1, D and E). Furthermore, immunofluorescence and confocal microscopy analysis of Caco2 monolayers revealed localization of all three LMO7, LIMCH1, and PDLIM1 distinctly to the apical ZA, similar to AGO2 localization, as determined by colocalization with mature Ecad adhesions and the ZA-specific marker PLEKHA7 (Kourtidis *et al.*, 2015, 2017b; Figure 1, F and G). Conversely, neither of these LIM proteins, AGO2, nor PLEKHA7, localize at basolateral areas of cell–cell contact (Figure 1, F and G). Together, these data point to the ZA as the subcellular compartment where PLEKHA7, AGO2, LMO7, LIMCH1, and PDLIM1 colocalize and interact; we also identify LIMCH1 and PDLIM1 as new ZA-associated LIM protein family members.

PLEKHA7, LMO7, LIMCH1, and PDLIM1 are required for recruitment of AGO2 to the ZA

We have shown that AGO2 localization at the ZA depends on PLEKHA7 (Kourtidis *et al.*, 2017b). Because LMO7, LIMCH1, and PDLIM1 interact with PLEKHA7 and AGO2 and all these proteins colocalize at the ZA, we asked whether any of these LIM proteins mediate recruitment of AGO2 to the ZA. Strikingly, shRNA-mediated knockdown of each of these LIM proteins resulted in loss of junctional AGO2 localization, without affecting AGO2 overall levels or cytoplasmic distribution, similarly to the effects of CRISPR/Cas9-generated PLEKHA7 knockout (KO; Figure 2, A–D) and of our published PLEKHA7 shRNA-mediated knockdown (Kourtidis *et al.*, 2017b). We also obtained identical results on AGO2's junctional localization in PLEKHA7, LMO7, LIMCH1, or PDLIM1 – depleted cells, by using an exogenously introduced Flag-tagged AGO2 construct (AGO2-Flag; Supplemental Figure S1, A–D), as well as by using a second, independent, set of LMO7, LIMCH1, and PDLIM1 shRNAs (Supplemental Figure S1, E–G). Furthermore, RNA immunoprecipitation and subsequent qRT–PCR analysis showed that LMO7, LIMCH1, or PDLIM1 knockdown resulted in decreased AGO2 loading of a set of miRNAs, namely miR-24, miR-200c, and miR-203a (Figure 2E). We have previously shown that PLEKHA7 depletion results in decreased AGO2 loading of the same set of miRNAs, which is an indicator of decreased AGO2 activity (Kourtidis *et al.*, 2017b). Interestingly, knockdown of neither LMO7, and LIMCH1, nor PDLIM1 had any effect on the localization or overall cellular levels of PLEKHA7 (Figure 2, C and D), suggesting that LIM protein-mediated effects on AGO2 are downstream of PLEKHA7. Based on these findings, we hypothesized that PLEKHA7 KO would result in loss of junctional localization of these proteins, leading to loss of junctional AGO2. Intriguingly, junctional localization of neither LMO7, and LIMCH1, nor PDLIM1 is affected by PLEKHA7 loss (Figure 3A). Similarly, in each of the three LIM protein knockdowns, junctional localization of the other two LIM proteins was also not affected (Figure 3, B–D), although knockdowns of all three LMO7, LIMCH1, and PDLIM1 result in loss of junctional AGO2. Taken together, these results indicate that although PLEKHA7, LMO7, LIMCH1, and PDLIM1 form a complex at the ZA (Figure 1, D–G) and are each individually required for recruitment of AGO2 to the ZA, their impact on AGO2 recruitment is independent of their complex formation and junctional recruitment. This suggests the existence of a downstream effector linked to all these proteins that regulates AGO2 recruitment to the junctions, which we sought to identify next.

PLEKHA7, LMO7, LIMCH1, or PDLIM1 depletion disrupts actomyosin organization at the ZA

LMO7, LIMCH1, and PDLIM1 have been previously reported to be involved in actomyosin organization (Bauer *et al.*, 2000; Vallenius *et al.*, 2000; Ooshio *et al.*, 2004; Tamura *et al.*, 2007; Maeda *et al.*, 2009; Lin *et al.*, 2017). We have also shown that PLEKHA7 knockdown

FIGURE 2: LMO7, LIMCH1, PDLIM1, and PLEKHA7 loss each disrupt junctional localization of AGO2. (A) Immunoblotting of PLEKHA7 KO Caco2 cells, compared with control wild-type cells (WT). (B) Immunofluorescence of control (WT) or PLEKHA7 KO cells for AGO2 and Ecad. AGO2 junctional fluorescence intensity normalized to cytoplasmic was quantified from $n = 30$ cell–cell junctions (10 junctions/field) representative of three independent experiments; statistical analyses were performed using unpaired two-way *t* test; $^{****}P < 0.0001$. (C) Immunoblotting of LMO7, LIMCH1, and PDLIM1 shRNA-mediated knockdown (shLMO7, shLIMCH1, shPDLIM1, respectively) Caco2 cells, compared with non-target (NT) shRNA control cells; asterisk indicates the specific LMO7 band lost by shRNA targeting. (D) Immunofluorescence of NT, shLMO7, shLIMCH1, and shPDLIM1 Caco2 cells for AGO2, PLEKHA7, and Ecad. AGO2 and PLEKHA7 junctional fluorescence intensity normalized to cytoplasmic was quantified from $n = 30$ cell–cell junctions (10 junctions/field) representative of three independent experiments; statistical analyses were performed using one-way ANOVA test; $^{****}P < 0.0001$; $^{*}P < 0.05$; ns, non-significant. Insets in all cases are marked by white rectangles and are 3× magnification of the original image. In all immunoblots, β-actin is the loading control; molecular masses (kD) are indicated on the right. Top-view immunofluorescence images were obtained by confocal microscopy and are single apical Z-slices. Scale bars = 20 μm. (E) AGO2 RNA immunoprecipitation (RNA IP) followed by qRT-PCR analysis for miR-24, miR-200c, and miR-203a miRNAs in NT, shLMO7, shLIMCH1, and shPDLIM1 Caco2 cells. Error bars represent mean ± SD from $n = 3$ independent experiments; statistical analysis was performed using one-way ANOVA $^{***}P < 0.005$; $^{**}P < 0.01$.

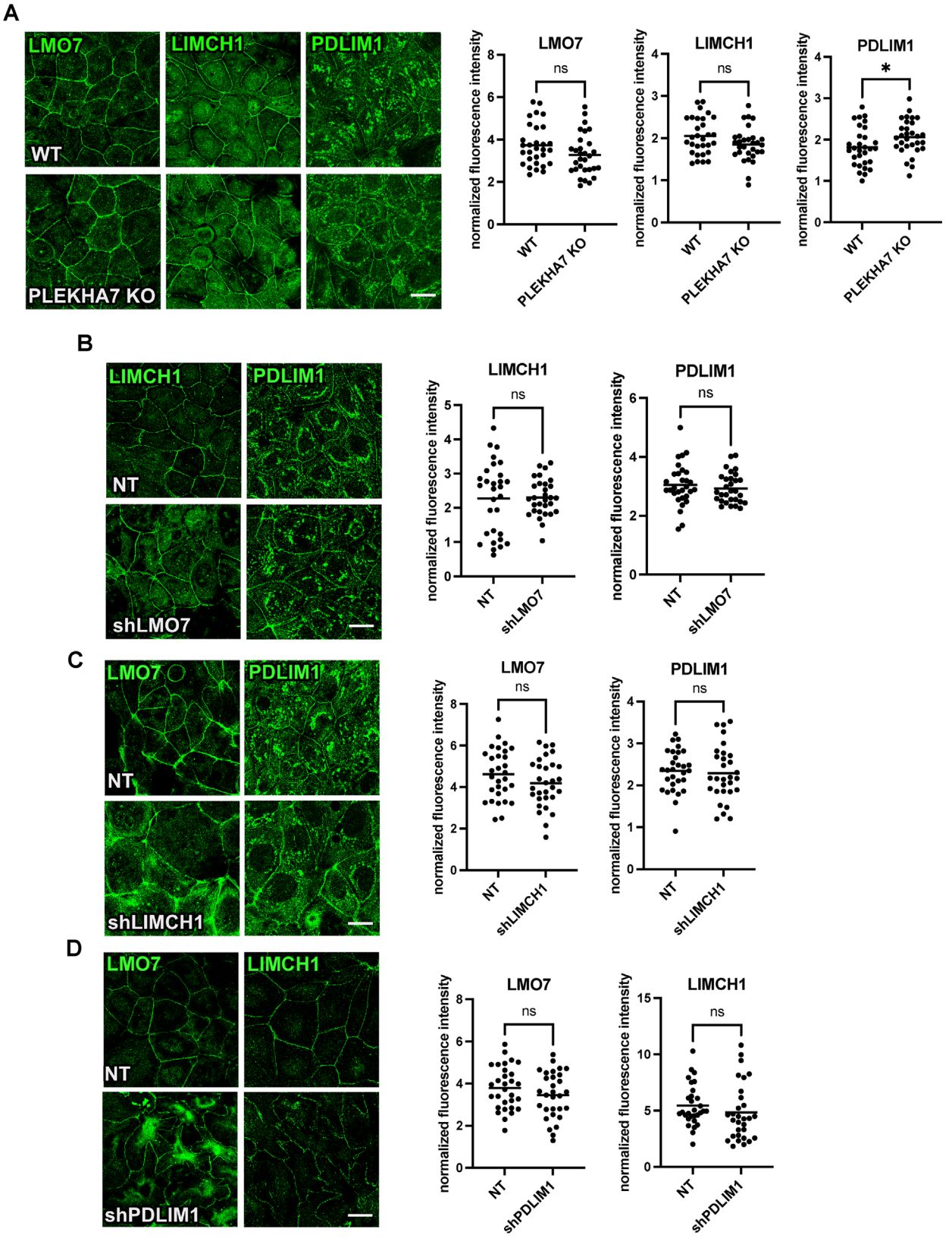

FIGURE 3: PLEKHA7, LMO7, LIMCH1, or PDLIM1 loss does not affect each other's localization to the junctions. (A) Immunofluorescence of control (WT) or PLEKHA7 KO cells for LMO7, LIMCH1, and PDLIM1. (B–D) Immunofluorescence of each LMO7, LIMCH1, and PDLIM1 in control (NT) and shLMO7, shLIMCH1, and shPDLIM1 Caco2 cells. For all figures, top-view immunofluorescence images were obtained by confocal microscopy and are single apical Z-slices. Junctional fluorescence intensity normalized to cytoplasmic was quantified from $n = 30$ cell–cell junctions (10 junctions/field) representative of three independent experiments; statistical analyses were performed using unpaired two-way *t* test; $^*P < 0.05$; ns, nonsignificant. Scale bars = 20 μm.

disrupts the integrity of the apical circumferential actin ring (Kourtidis *et al.*, 2015), and our GO analysis reveals actin-related functions are significantly enriched in the PLEKHA7-interacting proteome (Figure 1, A and B). Based on these observations, we asked whether the relationship of these components with the actin cytoskeleton could be the common denominator regulating AGO2 recruitment to the ZA. First, we examined potential effects of these proteins on actomyosin organization in Caco2 cells specifically at the ZA, where AGO2 is recruited. Using confocal and super resolution microscopy we found that PLEKHA7 KO cells exhibit disrupted actomyosin organization at the ZA, manifested by a disorganized circumferential actin ring and diffused junctional Myosin IIB (Figure 4A; Supplemental Figure S2A). Similarly, knockdown of each of LMO7, LIMCH1, and PDLIM1 had distinct, but in all cases significant effects on actomyosin organization throughout the cell and particularly at the ZA (Figure 4B; Supplemental Figure S2, B and C). More specifically, in LMO7 knockdown cells, apical actin filaments failed to tightly bundle into a dense cable as in control cells but remained loosely organized in dispersed, multifurcated, actin cables (Figure 4B). LIMCH1 knockdown cells showed a different pattern, where the apical filamentous actin ring is severely fragmented or completely absent (Figure 4B). Finally, PDLIM1 knockdown cells exhibited jagged actomyosin cables alongside bicellular junctions that appeared to be attached to intracellular actomyosin cables linked to dense cytoplasmic actomyosin aggregates (Figure 4B – bottom panel). This further manifested in wavy junctional cell borders and with the appearance of a distorted, collapsed apical ring structure (Figure 4B). Intense stress fibers were also observed in LMO7, LIMCH1, and PDLIM1 knockdown cells (Supplemental Figure S2B – basal panel). We particularly examined Myosin IIB to assess actomyosin organization, because this is the nonmuscle Myosin II isoform specifically responsible for contractile tension and actin filament stabilization at the apical actin ring at the ZA (Smutny *et al.*, 2010; Gomez *et al.*, 2015; Heuze *et al.*, 2019; Wayt *et al.*, 2021). Indeed, effects on Myosin IIA were not as consistent: although depletion of LMO7 and LIMCH1 resulted in disorganized and more diffused Myosin IIA, they also resulted in stronger Myosin IIA recruitment around areas of cell–cell contact, whereas depletion of PLEKHA7 or of PDLIM1 only minimally affected Myosin IIA recruitment at the ZA (Supplemental Figure S3, A and B). These results demonstrate that the negative effects of PLEKHA7, LMO7, LIMCH1, and PDLIM1 depletion on actomyosin organization at the ZA primarily involve Myosin IIB. Altogether, these results show that PLEKHA7, as well as LMO7, LIMCH1, and PDLIM1, are each distinctly responsible for the stability and homeostasis of the actomyosin cytoskeleton and particularly of the circumferential actin ring at the ZA.

AGO2 recruitment to the ZA depends on the presence of an organized actin cytoskeleton

Since PLEKHA7, LMO7, LIMCH1, and PDLIM1 are all required for stability of the apical actomyosin cytoskeleton and for recruitment of AGO2 to the ZA, independently of each other, we asked whether proper actin organization is the underlying mechanism mediating recruitment of AGO2 to the ZA. To examine this, we utilized a classical calcium-switch assay (Gumbiner and Simons, 1986) to dismantle the calcium-dependent Ecad-based junctions and allow them to recover with or without the presence of Latrunculin A (LatA), an actin polymerization inhibitor (Coue *et al.*, 1987; Figure 5A). Ecad-based junctions and the junctional localization of PLEKHA7 and AGO2, although entirely lost upon calcium depletion, fully recover within 1 h of calcium reintroduction in control cells (Figure 5, B–D). We also observe the same recovery time for the formation of a mature circumferential actin ring in these control cells (Figure 5A). These cells are entirely rounded before recovery begins, due to loss of cell–cell adhesion and actin contraction, which is marked by cytoplasmic, perinuclear actin rings (Figure 5A). However, as previously reported (Ivanov *et al.*, 2004; Yu-Kemp *et al.*, 2022), LatA-treated cells fail to round following calcium depletion, due to the lack of contraction, and pools of Ecad, as well as punctate actin pools, are retained at areas of cell–cell contact (Abe and Takeichi, 2008; Cavey *et al.*, 2008; Yamada *et al.*, 2004; Tang and Brieher, 2012; Figure 5, A and D). Furthermore, Ecad repopulates areas of cell–cell contact to reform AJs during recovery in the LatA cells, although these cells do not contain filamentous actin, again in agreement with previous observations (Ivanov *et al.*, 2004; Tang and Brieher, 2012; Yu-Kemp *et al.*, 2022; Figure 5, A and D). Interestingly, we also found that PLEKHA7 follows a similar pattern as Ecad in the LatA cells, mostly recovering at the junctions within 1 h of calcium reintroduction (Figure 5C). Therefore, although PLEKHA7 is critical for the stability of the actin cytoskeleton, its localization to the junctions does not depend on the presence of organized, filamentous actin. Notably, pools of LMO7, LIMCH1, and of PDLIM1 are also retained at cell–cell junctions upon recovery in the LatA-treated cells (Figure 5, E–H). However, localization of AGO2 to the junctions is completely abolished in LatA-treated cells and never recovers after calcium readdition (Figure 5, B and H). We obtained identical results using the AGO2-Flag construct (Supplemental Figure S4A). These data, together with our observed effects on actin organization and AGO2 ZA recruitment by each one of PLEKHA7, LMO7, LIMCH1, and PDLIM1, demonstrate that AGO2 recruitment to the ZA depends on the presence of an organized, mature apical actin ring, downstream of all four: PLEKHA7, LMO7, LIMCH1, and PDLIM1.

PLEKHA7, LMO7, LIMCH1, or PDLIM1 depletion disrupts mechanical tension at the ZA

Our findings demonstrate that AGO2 recruitment to the ZA depends on the presence of a mature circumferential actin ring and on PLEKHA7, LMO7, LIMCH1, and PDLIM1, which are all required for the stability of the actin cytoskeleton. However, we also noted that depleting each of these components had varied effects on apical actomyosin; apical actin filaments were present but dispersed in LMO7 and PDLIM1 knockdown cells (Figure 4B), whereas apical actin was fragmented and disorganized in LIMCH1 knockdown and PLEKHA7 KO cells (Figure 4, A and B). In most cases, apical actin was also notably dissociated from myosin. This is informative, because myosin monomers assemble to form an ATPase-powered motor that imposes contractile forces on the AJ-associated actin cytoskeleton (Vicente-Manzanares *et al.*, 2009). The dissociation of apical actin and myosin in the LIM knockdown and in PLEKHA7 KO cells, points to decreased F-actin mechanical tension (Uyeda *et al.*, 2011). To evaluate the effects of PLEKHA7, LMO7, LIMCH1, and PDLIM1 on contractile tension of the apical actin ring, we used the tension-sensitive α18 antibody, which recognizes an α-catenin epitope that becomes exposed when structural changes are induced by actomyosin tension (Yonemura *et al.*, 2010). Indeed, depletion of each of PLEKHA7, LMO7, LIMCH1, and PDLIM1 disrupted actomyosin tension at the ZA, as indicated by decreased α18 intensity at bicellular junctions, although total junctional α-catenin remained unaffected (Figure 6, A–D). Notably, each of these cell populations display distinct cell shape changes, further reflecting disruption of tension distribution (Levayer and Lecuit, 2012). More specifically: A) LMO7 knockdown cells are uneven in size, with either very large or small cells observed; B) LIMCH1 knockdown cells are uniformly large and flattened; and C) PDLIM1 knockdown cells are smaller

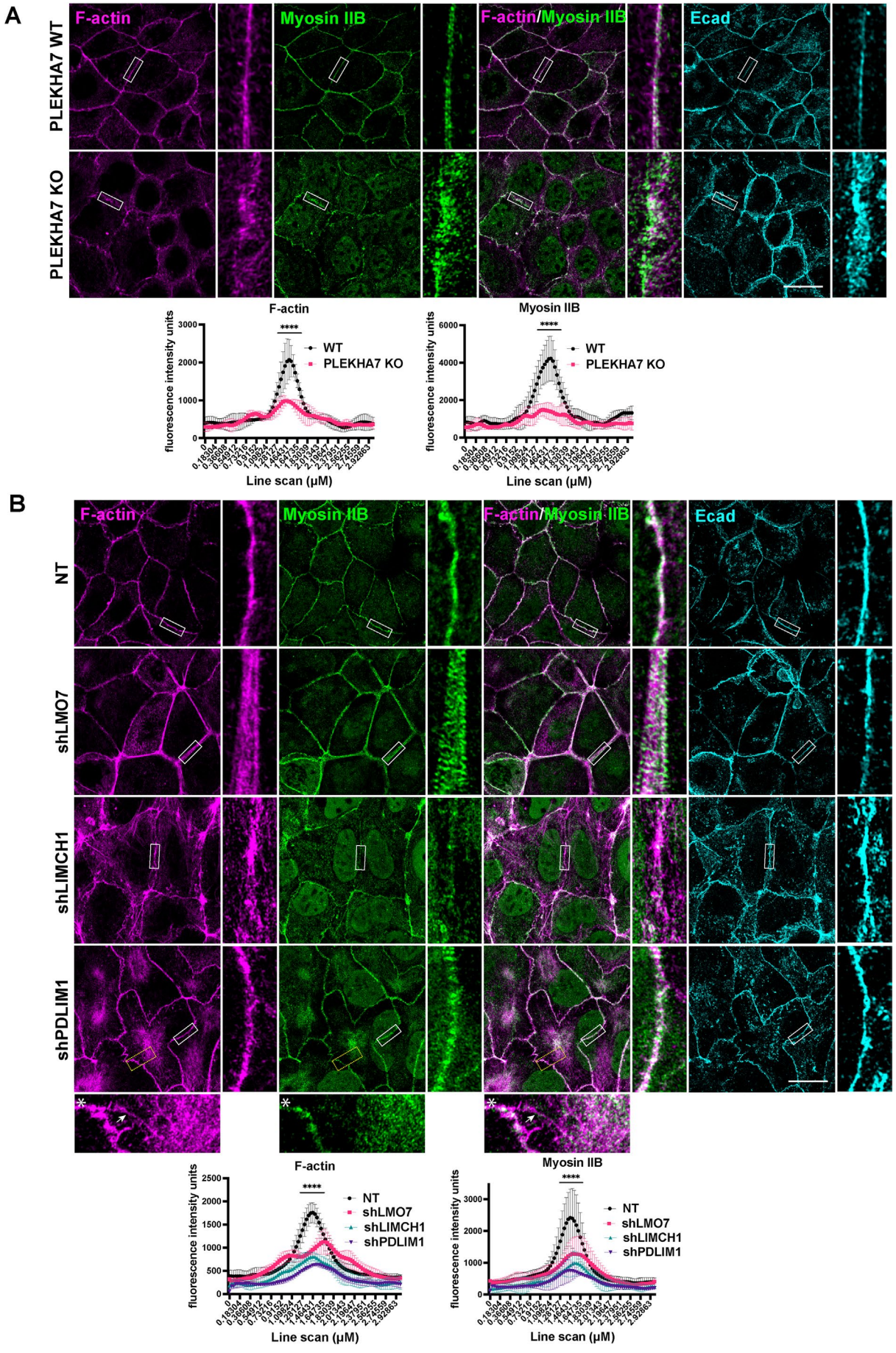
A
F-actin
Myosin IIB
F-actin/Myosin IIB
Ecad
PLEKHA7 WT
PLEKHA7 KO
F-actin
Myosin IIB
fluorescence intensity units
Line scan (μM)
****
WT
PLEKHA7 KO
B
NT
shLMO7
shLIMCH1
shPDLIM1

with distinct, wavy apical cell–cell borders (Figure 6C). Wavy apical cell–cell junctions, or otherwise loss of junction straightness, have also been previously associated with reduced contractile cortical tension on the junctions (Sumi *et al.*, 2018; Arnold *et al.*, 2019; Yamamoto *et al.*, 2021). Indeed, measurements of bicellular junction lengths show loss of junctional straightness in PDLIM1 knockdown cells (Figure 6E). Along these lines, depletion of each of PLEKHA7, LMO7, LIMCH1, and PDLIM1 also resulted in decreased phosphorylation of myosin II regulatory light chain at Serine 19 (pS19-MRLC), as well as in its uneven distribution along cell–cell junctions, further indicating disruption of actomyosin tension (Figure 6, F–I). Altogether, these results demonstrate that PLEKHA7, LMO7, LIMCH1, and PDLIM1 are all responsible for the establishment and proper distribution of tension at the ZA.

AGO2 recruitment to the ZA depends on actin tension and interaction with Myosin IIB at the ZA

We next asked whether contractile actomyosin tension at the ZA is also involved in the recruitment of AGO2 to the ZA. To examine this, we treated cells with: A) Blebbistatin, which inhibits the ATPase-dependent motor activity of myosin, but does not prevent its binding to actin (Kovacs *et al.*, 2004); or B) the ROCK inhibitor, Y-27632, which indirectly inhibits myosin II motor activity by preventing MRLC phosphorylation (Amano *et al.*, 2010). We performed these treatments during recovery, after calcium switch. Both Blebbistatin and Y-27632 resulted in decreased cortical actin ring tension, as indicated by disrupted actomyosin filaments and decreased α18 signals at the ZA (Supplemental Figure S4, B–D). Concomitantly, AGO2 junctional localization was also disrupted in cells with reduced contractile tension, when using both Blebbistatin and Y-27632, and as demonstrated by: A) loss of endogenous AGO2 localization to the ZA; B) loss of endogenous AGO2 colocalization to α18; C) loss of ZA localization of the ectopically expressed AGO2-Flag construct (Figure 7A; Supplemental Figures S4, E and F; and S5). Altogether, these results demonstrate that AGO2 localization at the ZA is sensitive to disruption of actin tension.

In contrast, PLEKHA7, LMO7, LIMCH1, and PDLIM1 localization to the ZA were unaffected by either Blebbistatin, or ROCK inhibition (Figure 7, B–F; and Supplemental Figure S5, B–F). Taken together with the LatA findings (Figure 5), and the PLEKHA7, LMO7, LIMCH1, and PDLIM1 depletion experiments (Figures 2 and 3), these results further demonstrate that the effects of PLEKHA7, LMO7, LIMCH1, or PDLIM1 depletion on AGO2 recruitment at the ZA are independent of either their junctional recruitment, or their protein–protein interactions, but rather associated with their downstream effects on actomyosin organization and tension. These results also suggest direct interaction of AGO2 with actomyosin. Because Myosin IIB was the actomyosin motor uniformly disrupted in all cases of PLEKHA7, LMO7, LIMCH1, and PDLIM1 depletion, we examined whether interaction with Myosin IIB mediates AGO2 localization at the ZA. Indeed, co-immunoprecipitation analysis revealed that AGO2 interacts with Myosin IIB (Figure 8A). We then implemented a proximity ligation assay (PLA) to assess whether this AGO2-Myosin IIB interaction particularly occurs at the ZA. We used the ectopically expressed AGO2-Flag construct for this assay to avoid any non-specific interactions with endogenous proteins and because we showed that this construct mimics the endogenous AGO2 by: A) identically localizing at the ZA; and B) this localization being similarly lost by LatA and Blebbistatin treatments in calcium switch assays (Supplemental Figures S1A and S4, A and F). Indeed, the AGO2-Flag:Myosin IIB PLA assay revealed interactions of AGO2 with Myosin IIB both at the ZA and the cytoplasm. However, the ZA-localized interactions were the ones that were specifically disrupted in all cases of PLEKHA7, LMO7, LIMCH1, and PDLIM1 depleted cells (Figure 8, B–E). In summary, our data demonstrate that actomyosin organization and tension at the ZA is the common downstream effector of all four PLEKHA7, LMO7, LIMCH1, and PDLIM1 in mediating AGO2 recruitment to the ZA, through regulating its interaction with Myosin IIB.

DISCUSSION

We have previously demonstrated that all major complexes of the RNAi machinery, namely the microprocessor complex, the DICER complex, as well as the RISC, including its main enzymatic component AGO2, distinctly localize at apical areas of cell–cell contact in well-differentiated epithelial cells and tissues and more specifically at the mature apical AJs that form the ZA (Kourtidis *et al.*, 2015, 2017b; Nair-Menon *et al.*, 2020). We have also shown that this ZA-associated RNAi machinery recruits and regulates processing and silencing activity of a set of miRNAs that suppress protumorigenic phenotypes (Kourtidis *et al.*, 2015, 2017b). Moreover, we found that this ZA-specific localization is disrupted in tumors from patients (Kourtidis *et al.*, 2015; Nair-Menon *et al.*, 2020), further supporting the idea of a tumor-suppressing role of the ZA-associated RNAi machinery in cancer. However, a key fundamental question emerged from these findings: why are these complexes specifically present at the ZA of well-differentiated epithelial cells and tissues, to begin with?

To address this question, we set off in this work to better understand the mechanistic underpinnings of this junctional RNAi recruitment. In our previous work, we identified PLEKHA7 as the ZA-specific component responsible for recruitment of RNAi complexes to the junctions (Kourtidis *et al.*, 2015, 2017b; Nair-Menon *et al.*, 2020). However, it remained unclear how PLEKHA7 recruits these RNAi components to the ZA. Through re-examining the PLEKHA7 proteome, we identified a set of LIM domain – containing proteins, namely LMO7, LIMCH1, and PDLIM1, as novel PLEKHA7 binding partners at the ZA. These proteins attracted our attention, because other members of the same family of proteins have been identified in the past as responsible for recruitment of AGO2 to cytoplasmic

FIGURE 4: PLEKHA7, LMO7, LIMCH1, and PDLIM1 each distinctly influence apical actomyosin organization. (A) Immunofluorescence and super resolution microscopy of PLEKHA7 KO Caco2 cells compared with control wild-type (WT) Caco2 cells. (B) Immunofluorescence and super resolution microscopy of LMO7, LIMCH1, and PDLIM1 knockdown (shLMO7, shLIMCH1, and shPDLIM1) Caco2 cells, compared with control (NT) shRNA cells. Top-view immunofluorescence images are maximum intensity projections of the two most apical Z-slices. Insets marked by white rectangles are 6× magnification of the original image. Insets for shPDLIM1 cells noted with asterisks are magnified 5× from areas marked with yellow dashed boxes. Asterisk marked insets are from full maximum intensity projection images to indicate basolateral actin filaments linked to the apical actin ring (marked by white arrows). In all cases, Ecad is used as a co-stain denoting AJs. Fluorescence intensity of 3-μm line scans drawn perpendicular to cell–cell junctions was measured from $n = 30$ cell–cell junctions (10 junctions/field) representative of three independent experiments; statistical analyses were performed using two-way ANOVA tests; error bars represent mean ± SD; ****$P < 0.0001$. Scale bars = 20 μm.

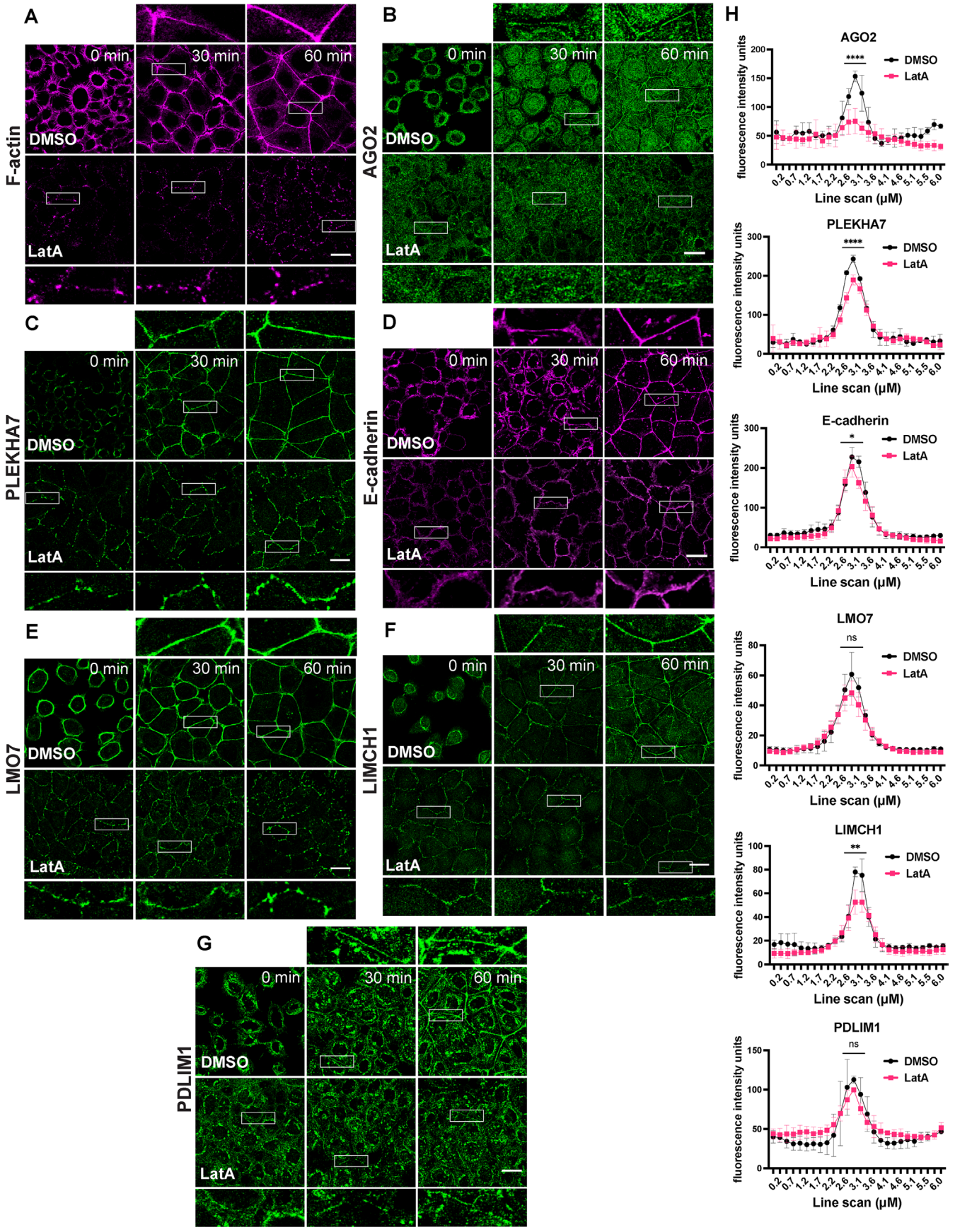
A
F-actin
0 min
30 min
60 min
DMSO
LatA
B
AGO2
C
PLEKHA7
D
E-cadherin
E
LMO7
F
LIMCH1
G
PDLIM1
H
AGO2
PLEKHA7
E-cadherin
LMO7
LIMCH1
PDLIM1
fluorescence intensity units
Line scan (μM)
****
*
**
ns
DMSO
LatA

p-bodies (James *et al*., 2010; Bridge *et al*., 2017; Tilley *et al*., 2020). Therefore, we examined the possibility that one of these proteins acts as the mediator between PLEKHA7 and AGO2 in recruiting it to the ZA. Surprisingly, we found that not only all three LMO7, LIMCH1, and PDLIM1 are equally and individually required for recruitment of AGO2 at the ZA and of its miRNA loading activity, as PLEKHA7 is, but also that this recruitment is independent of their interactions, either between them or with PLEKHA7, at the ZA. Instead, what our experimentation revealed is that all four PLEKHA7, LMO7, LIMCH1, and PDLIM1 are responsible for the stability of the actomyosin cytoskeleton at the ZA. We also found that this actomyosin stability, and more specifically the formation and maintenance of a mature, organized, tensile circumferential actin ring at the ZA, is the common denominator downstream of all four components that is responsible of AGO2 recruitment to the ZA. These findings have three major implications.

First, they explain why AGO2 is specifically recruited to apical cadherin junctions at the ZA but not at basolateral areas of cell–cell contact, as we previously demonstrated both in cells (Kourtidis *et al*., 2017b) and in tissues (Nair-Menon *et al*., 2020) and further confirm in this study (Figure 1, F and G). Although we have demonstrated this localization so far in colon and kidney epithelial cells (Caco2; MDCK; Kourtidis *et al*., 2017b) and in normal colon tissues (Nair-Menon *et al*., 2020), our current findings allow us to make the prediction that junctional AGO2 and its ensuing miRNA regulation may also be found in other epithelial cells and tissues that are well-differentiated and exhibit a mature, tensile circumferential apical actin ring and mature ZA. A similar prediction can be made not only when referring to human epithelia, but also to epithelia from other species, especially when considering that we have already seen this localization in at least one more species (canine MDCK cells). Because we have shown that PLEKHA7 is vertebrate-specific and has no invertebrate orthologue (Kourtidis *et al*., 2022), it would be particularly interesting to examine whether junctional AGO2 exists in invertebrate species, for example, by virtue of LMO7, which has invertebrate orthologues (Beati *et al*., 2018), or other similar actin-binding components. It remains to be seen whether these predictions will be confirmed in future studies.

Second, our findings suggest that any perturbations of the circumferential actin ring, which can occur during normal processes, such as tissue morphogenesis and junctional remodeling, or aberrantly, during disease, can disrupt AGO2 localization and function. For example, it is known that aberrant actin remodeling is common in cancer (Hayward *et al*., 2021), and we have shown that junctional localization of AGO2 is broadly lost in colon tumors and cancer cell lines (Nair-Menon *et al*., 2020). These findings suggest that the mechanism instructing association of AGO2 to the ZA is much broader than any single protein-directed interactions and reveal an underlying cellular mode of regulation that is more fundamental in nature. Corroborating this notion, we show here that depletion of any one of PLEKHA7, LMO7, LIMCH1, and PDLIM1 leads to disruption of both structure and tension of the apical actomyosin ring and in loss of AGO2 junctional localization and miRNA-loading ability. Therefore, mutations or downregulation of any of these components, or of many more actin-regulating proteins, may feed into the same mechanism as a common central node of regulation, promoting disease progression.

Thirdly, this work provides a conceptual framework, which can guide us to further study this localized RNAi function and to fully realize its physiological significance, because we have shown that the ZA-localized RNAi machinery is critical for processing and function of a set of miRNAs that regulate cell behavior (Kourtidis *et al*., 2015, 2017b; Nair-Menon *et al*., 2020). In this framework, RNAi complexes at the ZA act as sensors of actomyosin contractility and organization, directly linking the mechanical state of the cell with post-transcriptional regulation of gene expression and consequently rapid modulation of cell behavior. Although more experimentation is needed to fully establish this idea, these findings introduce the concept of "mechanosensitive RNAi." In this report, we focus specifically on AGO2, however, we can also apply this approach to study the other RNA-binding proteins and complexes that we have identified at the ZA (Kourtidis *et al*., 2015, 2017b) and to fully reconstruct their regulation and roles in cell and tissue homeostasis and disease. For example, we have recently shown that different extracellular matrix (ECM) components distinctly impact localization and complex formation of RNAi components to the ZA, including not only RISC and AGO2, but also DROSHA and the microprocessor (Daulagala and Kourtidis, 2022). It is well-established that different ECM components exert different mechanical forces in cells, which are primarily transmitted through the actomyosin cytoskeleton (Janmey *et al*., 2020). In light of our current findings, we can also make the prediction that these ECM-mediated effects on junctional recruitment and complex formation of RNAi complexes are indeed mediated through fine-tuning of the actin cytoskeleton, which remains to be tested in future studies.

Beyond its potential significance for the physiological relevance of the junctional AGO2 and RNAi, our findings may have additional repercussions on our understanding of the physiological roles of RNAi and miRNAs. For example, the actomyosin cytoskeleton has been implicated in localization and assembly of RNA-binding complexes in other cellular compartments, such as p-bodies in the cytoplasm or Cajal bodies and the RNA-induced transcriptional gene silencing-like (RITS-like) complex in the nucleus (Skare *et al*., 2003; Lindsay and McCaffrey, 2011; Ahlenstiel *et al*., 2012; McCaffrey and Lindsay, 2012). Furthermore, a more recent study showed that AGO2 in endothelial cells and fibroblasts engages miRNAs that particularly regulate biomechanical proteins and pathways, in response to being plated on stiff substrates (Moro *et al*., 2019). The above, taken together with our current findings, suggest that RNAi and miRNAs may indeed be a means for the cell to rapidly respond to biomechanical

FIGURE 5: AGO2 recruitment to the ZA depends on filamentous actin integrity. (A–G) Immunofluorescence of Caco2 cells for F-actin, PLEKHA7, AGO2, E-cadherin, LMO7, LIMCH1, and PDLIM1, fixed at indicated time points throughout a calcium switch assay. Images at 0 min indicate Ca^{2+} depleted cells immediately before Ca^{2+} reintroduction and at 30- and 60-min time points are following Ca^{2+} re-addition. Cells were pretreated and maintained in either DMSO vehicle (control) or 10 μM LatA throughout the calcium switch assay. Insets are marked by white rectangles and are 3× magnification of the original image. Scale bars = 20 μm. (H) Fluorescence intensity of 6-μm line scans drawn perpendicular to cell–cell junctions was measured for each marker at the 60-min time point upon recovery from n = 30 cell–cell junctions (10 junctions/field) representative of three independent experiments; statistical analyses were performed using two-way ANOVA tests; error bars represent mean ± SD; ****$P < 0.0001$; **$P < 0.01$; *$P < 0.05$; ns, non-significant.

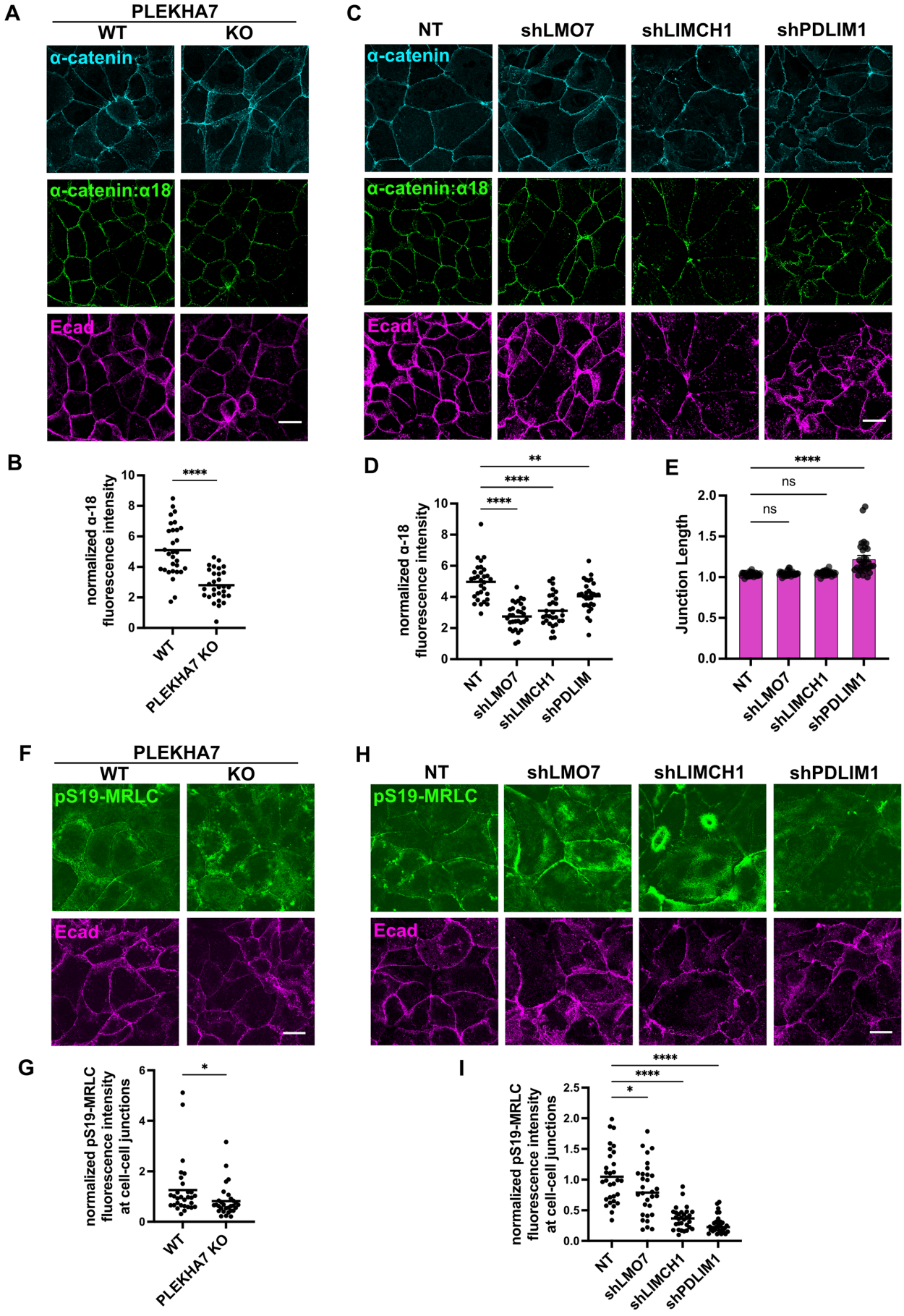
A
PLEKHA7
WT
KO
α-catenin
α-catenin:α18
Ecad
B
normalized α-18 fluorescence intensity
****
WT
PLEKHA7 KO
C
NT
shLMO7
shLIMCH1
shPDLIM1
α-catenin
α-catenin:α18
Ecad
D
normalized α-18 fluorescence intensity
**
****
****
NT
shLMO7
shLIMCH1
shPDLIM
E
Junction Length
****
ns
ns
NT
shLMO7
shLIMCH1
shPDLIM1
F
PLEKHA7
WT
KO
pS19-MRLC
Ecad
G
normalized pS19-MRLC fluorescence intensity at cell-cell junctions
*
WT
PLEKHA7 KO
H
NT
shLMO7
shLIMCH1
shPDLIM1
pS19-MRLC
Ecad
I
normalized pS19-MRLC fluorescence intensity at cell-cell junctions
****
****
*
NT
shLMO7
shLIMCH1
shPDLIM1

stimuli, further supporting the concept of "mechanosensitive RNAi" as a broader mechanism regulating cellular plasticity.

The present work also provides new information for the potential cellular functions of PLEKHA7, LMO7, LIMCH1, and PDLIM1. More specifically, we show that LMO7, LIMCH1, and PDLIM1 all coexist as a complex at the apical ZA, together with PLEKHA7 and AGO2. Localization of LMO7 at apical AJs has been previously reported (Ooshio *et al.*, 2004; Matsuda *et al.*, 2022), but not that of LIMCH1 and PDLIM1, because previous studies primarily focused on their roles in localizing with and modulating stress fibers (Bauer *et al.*, 2000; Vallenius *et al.*, 2000; Tamura *et al.*, 2007; Maeda *et al.*, 2009; Lin *et al.*, 2017). Then, we reveal that LMO7, LIMCH1, and PDLIM1 all regulate AGO2 recruitment to the ZA and miRNA loading to AGO2, identically to PLEKHA7 (Figure 2; Kourtidis *et al.*, 2017b). We also show that all four PLEKHA7, LMO7, LIMCH1, and PDLIM1 regulate actomyosin stability, albeit in seemingly different ways and potentially through different mechanisms. Using super-resolution microscopy, we show that PLEKHA7 depletion results in disruption of the actomyosin structure at the ZA, adding to our previously published findings showing that PLEKHA7 depletion results in cofilin activation and actin ring disruption (Kourtidis *et al.*, 2015; Kourtidis and Anastasiadis, 2016). Furthermore, our PLEKHA7 proteomics analysis identified high enrichment in actin-binding proteins (Figure 1, A and B), which builds on our previous work that revealed association of PLEKHA7 with certain components of the actin cytoskeleton, such as ACTN1 and MYL6 (Kourtidis and Anastasiadis, 2016). A recent study also demonstrated that PLEKHA7 is linked to Myosin IIB through CGLN1 (Rouaud *et al.*, 2023), which could also explain the effects of PLEKHA7 depletion on Myosin IIB distribution and actomyosin tension. We also show that LMO7 depletion negatively impacts actomyosin organization by resulting in a multifurcated apical actomyosin ring and extended, widened apical myosin arrays, an appearance previously described as "sarcomeric" (Choi *et al.*, 2016; Yu-Kemp *et al.*, 2022). This actomyosin organization is indicative of incomplete maturation of apical actin bundles (Choi *et al.*, 2016; Yu-Kemp *et al.*, 2022). In addition, LMO7-depleted junctions seem to be uneven in size and are less tensile. It has been shown that *Drosophila melanogaster* mutants lacking expression of Smallish (Smash), the fly orthologue of LMO7, also showed junctions of unequal shape in the larval epidermis, whereas *Drosophila* Smash or *Xenopus* LMO7 overexpression resulted in increased apical constriction, further supporting a conserved role for LMO7 in promoting actomyosin contractility (Beati *et al.*, 2018; Matsuda *et al.*, 2022). We also observed actomyosin disruption, increased cell spreading and decreased contractility in LIMCH1 knockdown cells, similarly to what was previously reported in stress fibers in HeLa cells (Lin *et al.*, 2017). Strikingly, our PDLIM1-depleted cells exhibited a notably distinct phenotype, with distorted cell borders that resemble those observed when the cortical actomyosin-associated protein Merlin is depleted in Caco2 cells (Chiasson-MacKenzie *et al.*, 2015). This phenotype was associated with increased contraction of the medioapical cortical cytoskeleton and reorientation of pulling forces inward, perpendicular to cell–cell junctions (Chiasson-MacKenzie *et al.*, 2015), contrasting contraction of the circumferential actomyosin belt, which exerts pulling forces parallel to the bicellular junctions. This loss of parallel junctional tension, coupled with increased medioapical contraction, has been associated with the presence of F-actin bundles linked perpendicular to the junctions (Arnold *et al.*, 2019), which we also noted in PDLIM1 knockdown cells (Figure 4B). Altogether, these observations strongly support critical and distinct roles of LMO7, LIMCH1, and PDLIM1 on actomyosin stability at epithelial ZA. However, the molecular details of these roles remain to be thoroughly investigated in subsequent studies.

In conclusion, our study demonstrates that AGO2 recruitment and function at epithelial cell–cell junctions responds to the presence of a structurally mature and mechanically tensile actomyosin cytoskeleton at the ZA, introducing the concept of "mechanosensitive RNAi". Our findings also suggest that this mechanosensitive RNAi may be a broader, more fundamental property of the cell, adding another layer of regulation of cellular plasticity, which can have implications in our understanding of developmental or diseased processes.

MATERIALS AND METHODS

Request a protocol through *Bio-protocol*.

Cell culture, constructs, and generation of stable cell lines

In all comparisons, cells were used at strictly the same confluencies. All cell lines were authenticated by the University of Arizona Genetics Core (via Science Exchange) and checked for misidentified, cross contaminated, or genetically drifted cells. Cell lines tested negative for mycoplasma contamination (LookOut Mycoplasma PCR Detection Kit, Sigma Aldrich). Caco2 colon epithelial cells (ATCC, #HTB-37) were cultured in MEM (Corning) supplemented with 10% fetal bovine serum (FBS; Life Technologies), 1 mM sodium pyruvate (Life Technologies), and 1× non-essential amino-acids (NEAA) solution (Life Technologies). HEK 293FT human embryonic kidney cells (Thermo Fisher Scientific, #R70007) were cultured in DMEM (Corning) supplemented with heat-inactivated 10% FBS, 2 mM additional L-glutamine, 1 mM sodium pyruvate, and 1× NEAA. Cells were maintained at 37°C with 5% CO_2. Lentiviral shRNA constructs were derived from the pLKO.1-based TRC1 shRNA library (Sigma-Aldrich/RNAi Consortium); the following vectors were used: pLKO.1-puro Non-Target shRNA Control, SHC016; shLMO7, TRCN0000006491; shLIMCH1, TRCN0000153799; shPDLIM1, TRCN0000161271; 2nd set: shLMO7, TRCN0000006492; shLIMCH1, TRCN0000154280; shPDLIM1 TRCN0000163210. The pLJM1-FLAG-HA-AGO2-WT (Addgene plasmid # 91978; http://n2t.net/addgene:91978; RRID:Addgene_91978) and pLJM1-Empty (Addgene plasmid # 91980; http://n2t.net/addgene:91980; RRID:Addgene_91980) lentiviral vectors were a gift from Joshua Mendell (Golden *et al.*, 2017). Lentiviral particles were produced in HEK 293FT cells co-transfected via Lipofectamine 2000 (Invitrogen)

FIGURE 6: Contractile tension at the ZA is disrupted in LMO7, LIMCH1, PDLIM1 knockdown and PLEKHA7 KO cells. Immunofluorescence of (A–E) total, as well as of tensile α-catenin using the α18 antibody that recognizes α-catenin upon tension, as well as of (F–I) phosphorylated myosin light chain at S19 (pS19-MRLC) that also indicates tension, in wild-type (WT) or PLEKHA7 KO Caco2 cells and in control (NT) or LMO7, LIMCH1, and PDLIM1 knockdown (shLMO7, shLIMCH1, and shPDLIM1) cells. Ecad is used as a co-stain denoting AJs. α18 fluorescence intensity measurements were normalized to total α-catenin (B and D) and pS19-MRLC were normalized to Ecad (G and I). All quantifications are from $n = 30$ cell–cell junctions (10 junctions/field) representative of three independent experiments. Statistical analyses were performed using unpaired two-way *t* tests (B and G) or one-way ANOVA tests (D, E, and I). ****$P < 0.0001$; **$P < 0.01$; *$P < 0.05$; ns, non-significant. Scale bars = 20 μm.

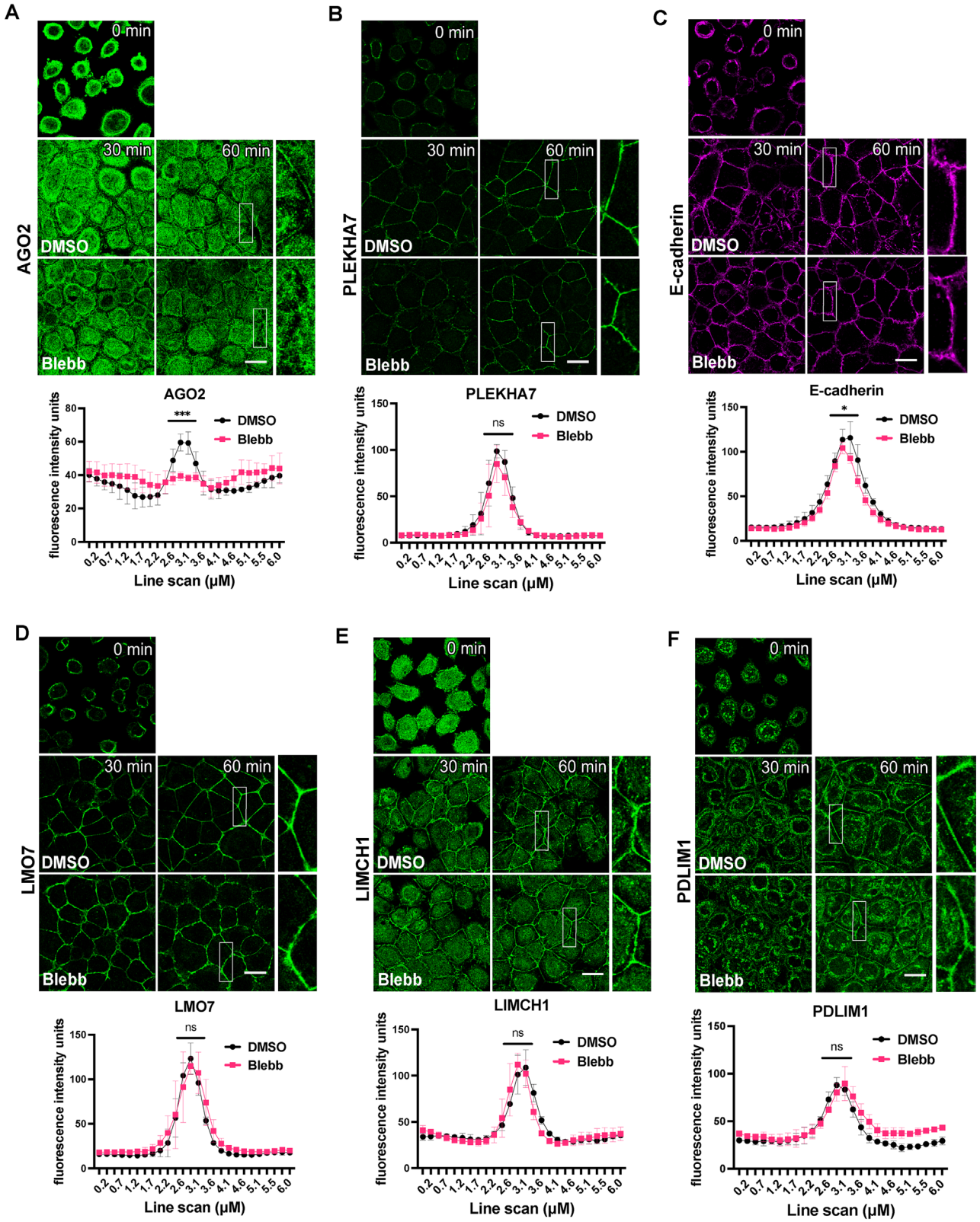

FIGURE 7: Contractile actin tension at the ZA is required for AGO2 junctional recruitment. (A–F) Immunofluorescence of Caco2 cells during a calcium switch assay in which DMSO or Blebbistatin (Blebb) were included in the calcium-containing recovery medium. Cells fixed at 30 and 60 min post Ca^{2+} reintroduction were stained for AGO2 (A), PLEKHA7 (B), E-cadherin (C), LMO7 (D), LIMCH1 (E), and PDLIM1 (F). Insets are marked by white rectangles and are 3× magnification of the original image. Fluorescence intensity of 6-μm line scans drawn perpendicular to cell–cell junctions was measured for each marker at the 60-min time point upon recovery from $n = 30$ cell–cell junctions (10 junctions/field) representative of three independent experiments; statistical analyses were performed using two-way ANOVA tests. Error bars represent mean ± SD. ****$P < 0.0001$; *$P < 0.05$; ns, non-significant. Scale bars = 20 μm.

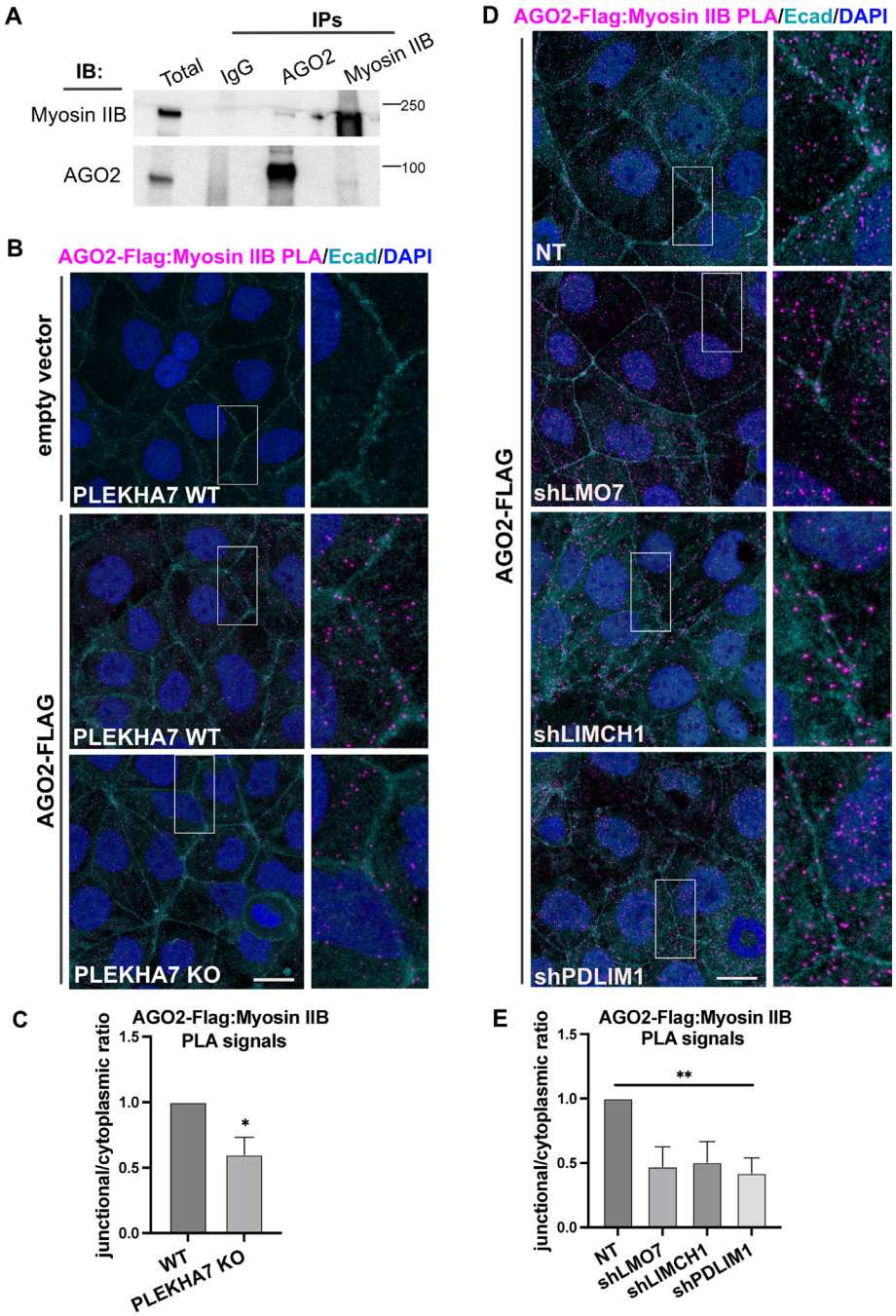

FIGURE 8: PLEKHA7, LMO7, LIMCH1, or PDLIM1 depletion each disrupt AGO2-Myosin IIB interaction at the ZA. (A) Immunoprecipitation (IP) of AGO2 and Myosin IIB from Caco2 cells, immunoblotted (IB) for the same markers; IgG is the negative control. Molecular masses (kD) are indicated on the right. (B–E) Wild type (WT) or PLEKHA7 KO Caco2 cells and control (NT) or LMO7, LIMCH1, and PDLIM1 knockdown (shLMO7, shLIMCH1, and shPDLIM1) cells stably expressing an AGO2-Flag construct (see Supplemental Figure S1, A–D) were subjected to PLA for AGO2-Flag, using an anti-Flag antibody, and Myosin IIB, followed by immunofluorescence staining for Ecad and confocal microscopy; DAPI was used to stain nuclei. Caco2 cells stably transduced with an empty vector were used as negative PLA control. Insets are marked by white rectangles and are 3× magnification of the original image. The ratio of junctional vs cytoplasmic PLA signals was quantified for each condition and from $n = 30$ cells (10 cells/field) representative of three independent experiments; statistical analyses were performed using either unpaired two-way *t* test (B–C) or one-way ANOVA test (D–E). Error bars represent mean ± SD. $^{**}P < 0.01$; $^{*}P < 0.05$. Scale bars = 20 μm.

with the shRNA vector and Virapower packaging plasmids (pMDLg/pRRE, Addgene #12251; pRSV-Rev, Addgene #12253; pMD2.G, Addgene #12259) according to manufacturer instructions. shRNA lentivirus was collected and used to infect Caco2 cells according to standard protocols. Stable shRNA-expressing cell lines were maintained in 2.5 μg/ml puromycin (Life Technologies) following initial selection at 5 μg/ml.

The PLEKHA7 KO Caco2 cell line was generated using CRISPR/Cas9 technology, as previously described (Ran *et al.*, 2013). The sgRNA sequence (GGATGTTTCACTGACCATGCTGG) targeting exon 5 of PLEKHA7 was designed using the online Synthego tool (www.synthego.com) and synthesized by Integrated DNA Technologies, IDT. This PLEKHA7-targeting sgRNA was cloned into the PX459 pSPCas9(BB)-2A-Puro vector (Ran *et al.*, 2013). Caco2 cells were transfected with 30 μg the sgRNA-containing vector using Lipofectamine 3000 (Invitrogen) according to the manufacturer's protocol. After 24 h, cells were selected with 5 μg/ml puromycin for 48 h. Successfully transfected cells were seeded to obtain single colonies, which were picked and expanded for screening. PCR using primers designed to amplify the target region (Forward: CCTTTCTCAGGGCCTCATGTCA; Reverse: GCCTCCAAACAATCAGGGTTGG) was performed with DNA extracted from colonies using QuickExtract (Lucigen). PCR amplified products were screened by restriction digest analysis using the CviAII restriction enzyme (New England Biolabs). Positive candidates were sequenced to identify and confirm indels (Supplemental Figure S6).

Antibodies

The primary antibodies used in this study were PLEKHA7 (HPA038610; Sigma-Aldrich), Ecad (610182; BD Transduction Labs), AGO2 (ab57113; Abcam - optimal for immunoblotting), AGO2 (AP5281; ECM Biosciences - optimal for immunofluorescence), AGO2 (ab156870; Abcam - optimal for immunofluorescence and immunoprecipitation/RNA- immunoprecipitation); LMO7 (ab224113; Abcam), LIMCH1 (ab96178; Abcam), PDLIM1 (ab129015; Abcam), β-actin (4967L; Cell Signaling Technology), Myosin IIB (909901; Biolegend), Myosin IIA (909801; Biolegend), pS19-MRLC (3671; Cell Signaling Technology), α-catenin (610193; BD Transduction Labs), anti-Flag (clone M2, F1804; Sigma-Aldrich). Working dilutions were 1:50 to 1:500 for immunofluorescence

and 1:500 to 1:2000 for Western blot. One exception was the polyclonal α-catenin (α18) antibody (Yonemura *et al.*, 2010), which was a gift from Dr. Akira Nagafuchi (Nara Medical University, Japan), used at 1:4000 for immunofluorescence.

The secondary antibodies used in the present study were HRP anti–mouse (711-035-150; Jackson ImmunoResearch Laboratories), HRP anti–rabbit (711-035-152; Jackson ImmunoResearch Laboratories), Clean-Blot HRP IP Detection Reagent (21230; Thermo Fisher Scientific), Alexa Fluor 488 anti–mouse (A21202, A11029; Invitrogen), Alexa Fluor 488 anti–rabbit (A21206, A11034; Invitrogen), Alexa Fluor 488 anti–rat (A11006; Invitrogen), Alexa Fluor 594 Phalloidin (A12381; Invitrogen), Alexa Fluor 647 anti–mouse (A21236; Invitrogen), Alexa Fluor 647 anti–rabbit (A21245; Invitrogen). Working dilutions were 1:500 for immunofluorescence and 1:2000 for Western blot. Exceptions included: Alexa Fluor 594 Phalloidin, used at 1:100 for immunofluorescence and Clean-Blot HRP used at 1:400 when blotting for PDLIM1 in IP-eluted samples.

Immunoprecipitation

Cells were grown on 10-cm plates until fully confluent, placed on ice, washed with ice-cold PBS, and lysed with ice-cold Triton X-100 lysis buffer (150 mM NaCl, 1 mM ethylenediaminetetraacetic acid (EDTA), 50 mM Tris, pH 7.4, and 1% Triton X-100) containing 2× protease (Protease Inhibitor Cocktail III, RPI) and phosphatase inhibitors (Halt Phosphatase Inhibitor Cocktail, Thermo Scientific). Six 10-cm plates were used per IP. Before cell lysis, 7 µg of antibody or IgG control (011-000-003; Jackson ImmunoResearch Laboratories) was incubated with 50 µl Protein G Dynabeads (Invitrogen) in 200 µl PBS with 0.02% Tween-20 for 10–12 h at 4°C with constant end-to-end rotation. For the AGO2 IP, 8 µg of antibody or IgG isotype control (ab18443; Abcam) were used. After washing the antibody-conjugated beads three times with immunoprecipitation (IP) lysis buffer, cell lysates were incubated with the bead-conjugated antibodies 12 h at 4°C with constant end-to-end rotation. Beads were then washed three times with IP lysis buffer and eluted using 50 mM dithiothreitol (DTT; Sigma-Aldrich) and 0.5% sodium dodecyl sulfate (SDS) in lysis buffer at 58°C for 30 min, with constant agitation. Eluted proteins were separated by SDS–PAGE and analyzed by immunoblotting as described below.

RNA immunoprecipitation (RNA-IP) and qRT-PCR

Cells were grown on 10-cm plates until fully confluent. Cells were then immediately placed on ice, washed once with sterile ice-cold PBS, and lysed with ice-cold, filter-sterilized, IP lysis buffer (150 mM NaCl, 1 mM EDTA, 50 mM Tris pH 7.4, 1% Triton X-100), containing 2× amount of protease (cocktail III, RPI) and phosphatase inhibitors (Pierce), as well as 100 U/ml RNAse Inhibitor (RNAsin; Promega). Cells were scraped, left for 20 min on ice and lysates were cleared up by full-speed centrifugation for 5 min at 4°C and precleared with Protein G Dynabeads (Life) for 1 h at 4°C with constant end-to-end rotation. Lysate from a total of 2 × 10 cm plates was used per IP. In parallel, 4 µg of rabbit AGO2 antibody (ab156870; Abcam) or rabbit IgG control (011-000-003; Jackson ImmunoResearch Laboratories) were incubated O/N with 40 µls Protein G Dynabeads (Invitrogen) in 300 µls sterile 1×PBS + 0.02% Tween and then washed 3× with IP lysis buffer. Pre-cleared lysates were incubated with the beads-conjugated antibodies for 12 h at 4°C with constant end-to-end rotation, with the exception of 100 µls that were kept at -20°C as the total lysate control. Beads were then washed 3× with ice-cold IP lysis buffer (sterile) and immunoprecipitated complexes were eluted using 100 µls elution buffer composed of: IP lysis buffer + 2× protease + 2× phosphatase inhibitors + 100U/ml RNAsin inhibitors + 50 mM DTT + 0.5% SDS (sterile) at 58°C for 30 min. Eluates were then transferred in fresh tubes and RNA extraction was performed by adding 500 µls Trizol (Invitrogen) and by using the Trizol Plus Total Transcriptome Isolation protocol of the PureLink RNA mini kit (Ambion – Life Technologies). Final RNA concentrations were determined using a BioDrop spectrophotometer. RNA was converted to cDNA using the High Capacity cDNA Reverse Transcriptase Kit (Applied Biosystems). qPCR reactions were performed using the Taqman FAST Universal PCR master mix (Applied Biosystems), in a BioRad CFX96 Touch/Connect real time quantitative PCR machine. Data were analyzed and normalized using the Sigma RIP-qRT-PCR Data Analysis Calculation Shell, associated with the Sigma Imprint RIP kit (www.sigmaaldrich.com/life-science/epigenetics/imprint-rna.html) and the references therein. TaqMan assays used (Applied Biosystems, catalogue# 4427975): hsa-miR-24, 000402; hsa-miR-200c, 002300; hsa-miR-203a, 000507.

Immunoblotting

Whole-cell extracts were obtained using RIPA buffer (50 mM Tris, pH 7.4, 150 mM NaCl, 1% NP-40, 0.5% deoxycholic acid, and 0.1% SDS) supplemented with protease and phosphatase inhibitors. Lysates were homogenized through a 29-G needle and cleared by full-speed centrifugation for 5 min. Protein quantification was performed using a Pierce BCA Protein Assay (Thermo Fisher Scientific). Protein extracts were mixed with Laemmli sample buffer and separated by SDS–PAGE using 4–20% Tris-Glycine eXtended (TGX) gels (Bio-Rad) and transferred to 0.2 µm nitrocellulose membranes (Bio-Rad) with the Trans-Blot Turbo Transfer System (Bio-Rad). Membranes were blocked and blotted in 3% milk according to standard protocols. Signals were detected by luminescence using Pierce ECL (Thermo Fisher Scientific) and a ChemiDoc Imaging System (Bio-Rad).

Immunofluorescence

Cells were grown in 12-well plates on 18 mm on sterile glass coverslips until they reached full confluence. Cells were washed once with PBS and fixed with either: A) 100% methanol (Thermo Fisher Scientific) at –20°C for 7 min; or B) 3.7% formaldehyde (Electron Microscopy Sciences) in PBS at RT for 20 min. Following 3.7% formaldehyde fixation, cells were washed three times with PBS + glycine (10 mM) and permeabilized for 7 min using 0.15% Triton X-100 in PBS. Cells counterstained with phalloidin to visualize F-actin were 3.7% formaldehyde fixed, while most all other cells were fixed with 100% methanol. Cells immunostained using the α18 antibody (Yonemura *et al.*, 2010) were fixed with 1% formaldehyde in 0.1M HEPES (Life Technologies) at RT for 20 min, washed three times with PBS + glycine (10 mM), and permeabilized for 12 min using 0.15% Triton X-100 in PBS.

Cells were blocked with serum free Protein Block reagent (Dako) at RT for 1hr and stained with primary antibodies diluted in Antibody Diluent (Dako) overnight at 4°C. Cells were then washed three times with PBS, stained with the fluorescent-labeled secondary antibodies for 1 h at RT, washed three times with PBS, costained with DAPI (Sigma-Aldrich), and mounted (Aqua-Poly/Mount; Polysciences).

Calcium switch and cytoskeletal inhibitor treatments

Caco2 cells were grown on coverslips until confluence. In LatA-treated calcium switch assays, cells were pretreated with either dimethyl sulfoxide (DMSO; Fisher Scientific) or 10 µM LatA (Thermo Fisher Scientific) for 10 min, washed three times with calcium-free PBS, and incubated in calcium-free Caco2 medium (S-MEM; Life Technologies), supplemented with glutamine, 10% FBS, sodium pyruvate, NEAA, and containing 4 mM ethylene glycol-bis(β-aminoethyl ether)-*N*,*N*,*N*′,*N*′-tetraacetic acid (EGTA) for 30 min, until cells were

rounded. Calcium-free EGTA-containing medium also contained either DMSO or 10 µM LatA. Cells were then washed three times with PBS, returned to regular Caco2 medium, again with either DMSO or LatA, and fixed for immunofluorescence at the indicated time points. In Blebbistatin or Y-27632-treated calcium switch assays, there was no pretreatment before incubation with calcium-free EGTA-containing Caco2 medium. Treatment was introduced in recovery, following cell rounding. In recovery, regular Caco2 medium contained either 50 µM (±)-Blebbistatin (Calbiochem)/DMSO control or 30 µM Y-27632 (Calbiochem)/water control. For static cytoskeletal inhibitor treatments, confluent cells were treated with 50 µM Blebbistatin for 3 h or 20 µM Y-27632 for 2 h.

Proximity Ligation Assay (PLA)

Confluent cells were fixed by using 4% paraformaldehyde (Electron Microscopy Sciences) and permeabilized with 0.2% Triton-X (Thermo Fisher Scientific) in PBS at room temperature. Coverslips were blocked using a blocking reagent (Dako) for 1 h at room temperature and probed with primary antibodies diluted in antibody diluent (Dako) overnight at 4°C. Primary antibodies used were anti-Flag (clone M2; F1804; Sigma-Aldrich) and Myosin IIB (909901; Biolegend) at 1:500 dilution. Coverslips were then washed with Duolink In Situ Wash Buffer-A (Sigma-Aldrich; DUO82049) and incubated with a Duolink Anti-Mouse plus PLA probe (Sigma-Aldrich) together with a Duolink Anti-Rabbit minus PLA probe (Sigma-Aldrich) at 37°C, for one hour, in a humidified chamber. Coverslips were then washed with Duolink In Situ Wash Buffer-A (Sigma-Aldrich), incubated with ligation solution (Sigma-Aldrich) for 30 min at 37°C, washed with Duolink In Situ Wash Buffer-A, and incubated with polymerase solution (Sigma-Aldrich) for 100 min at 37°C. Coverslips were then washed with Duolink In Situ Wash Buffer-B (Sigma-Aldrich), then with Duolink In Situ Wash Buffer-A and counterstained with Alexa fluor 488 conjugated Ecad antibody (3199S; Cell Signaling Technology) for 1 h at room temperature. Coverslips were eventually washed with Duolink In Situ Wash Buffer-B and with Duolink In Situ Wash Buffer-A before being mounted with Duolink In Situ Mounting Medium with DAPI (Sigma-Aldrich). Coverslips were imaged using a Leica SP8 confocal microscope under 63× objective with an additional 1.5× zoom, with Z-stack acquisition intervals at 0.5–1 µm, image resolution at 1024 × 1024 pixels, 600 Hz scan speed, and scan line average at four.

GO enrichment analysis

The full published dataset of the 607 PLEKHA7-interacting proteins (publicly available at www.imexconsortium.org/; identifier: IM-25739; Kourtidis *et al.*, 2017b) was analyzed using the GO Enrichment analysis online tool (http://geneontology.org; Ashburner *et al.*, 2000; Mi *et al.*, 2019; Gene Ontology, 2021). Annotation version and release date of the PANTHER database used was: Reactome version 65, released 2020-11-17. Statistical analysis was performed using the PANTHER Overrepresentation Test tool. Test type used was Fisher's exact test with false discovery rate (FDR) correction. Annotation datasets used for the analysis were the PANTHER GO-slim Molecular Function and the PANTHER GO-slim Biological Process.

Imaging, image processing, analysis, and statistics

Images were acquired using Leica SP5 and SP8 confocal microscopes with 63× Plan-Apochromat 1.4NA DIC oil immersion objectives (Leica) and 405 nm, 488 nm, 594 nm, and 633 nm lasers. Image acquisition was done using Leica Application Suite Advanced Fluorescence X software at 1024 × 1024 resolution and with 0.4 µm intervals along the z-axis. For super resolution imaging, Z-series stacks were acquired in 0.4 µm intervals on a Zeiss LSM 880 NLO Quasar point scanning confocal microscope using the Airyscan detector, a 63× Plan-Apochromat 1.4NA DIC oil immersion objective (Zeiss) and the 405 nm, 488 nm, 561 nm, and 633 nm laser lines at 2024 × 2024 resolution, with 1.8× zoom. The Zeiss Zen 2.3 (black edition) software was used to control the microscope, adjust spectral detection, and for processing of the Airyscan raw images.

To allow for comparison, the same imaging parameters were used across conditions for each set of experiments. Unless otherwise noted, images shown are single Z-slices. For quantifications of confocal and super resolution images, maximum intensity projections of the two most apical Z-slices were used to account for uneven cell thicknesses and ensure full representation of all apical cell–cell junctions throughout each field. Quantifications were done using Fiji (Schindelin *et al.*, 2012; National Institutes of Health). Individual borders for measuring signal intensity or junction straightness were manually and randomly selected based on apical signals, using apical Ecad as a reference in most cases. Integrated fluorescence intensity values were measured using Fiji from drawing either: A) 6 µm lines tracing cell–cell borders, when assessing junctional marker fluorescence intensity, normalized to fluorescence intensity averages of equal number of 6-µm lines drawn randomly throughout the cytoplasm, to account for staining fluctuations and/or total protein levels; B) 6 or 3 µm (e.g., for the super-resolution images) lines perpendicular to cell–cell borders, when assessing both fluorescence intensity, as well as distribution of this marker across cell–cell junctions; C) 8 × 3 µm boxes centered on cell–cell junctions when using the α18 antibody, to include jagged junctions. To measure junctional straightness, the length of a line tracing the cell border from one tricellular junction to the next was compared with the length of a straight line drawn directly from one tricellular junction to another.

For all measurements, sample size and related statistics are indicated in the respected figure legends. In general, we used: A) unpaired two-way *t* tests when comparing two groups; B) one-way ANOVA when comparing three or more groups; and C) two-way ANOVA when more than one parameters were considered (e.g., fluorescence intensity and distance). Statistics and graphs were all performed using Prism 10 (GraphPad). All experiments, including gene knockdowns and immunoprecipitation experiments, were performed in at least three independent experiments, unless otherwise noted, and representative images are shown.

ACKNOWLEDGMENTS

This work was supported by National Institutes of Health grants R01 DK124553, R21 CA246233, P20 GM130457, 3P20 GM130457-04S1, P30 DK123704, P20 GM103499-21S1, and UL1 TR001450 (Medical University of South Carolina, South Carolina Clinical & Translational Research Institute Discovery Grant), and P30 CA138313 (Hollings Cancer Center Pre-Clinical & Clinical Concepts Pilot Award) to A.K.. M.C.B. was supported by National Institutes of Health training grants TL1 TR001451 and UL1 TR001450. A.R. was supported by National Institutes of Health training grants TL1 TR001451, UL1 TR001450, and T32 5T32DK124191. A.D. was supported by the Abney Graduate Fellowship Award, Hollings Cancer Center (P30 CA138313), Medical University of South Carolina. C.K. was supported by National Institutes of Health training grant 5T32 DE017551.

We would like to thank Dr. Akira Nagafuchi, Nara Medical University, Japan, for kindly providing the α18 antibody; Drs. Christiana Kappler and Stephen Duncan, Cell Models Core, Medical University of South Carolina Center of Biomedical Research Excellence (COBRE) in Digestive & Liver Disease (CDLD; National Institutes of

Health P20 GM130457) and Medical University of South Carolina Digestive Disease Research Center (DDRC; National Institutes of Health P30 DK123704) for support with CRISPR/Cas9 reagents; Drs. Li Li and John Lemasters, Advanced Imaging Core, CDLD and DDRC (National Institutes of Health P20 GM130457 and P30 DK123704) for support with super resolution microscopy; Dr. David Turner and the shRNA Technology Shared Resource, Hollings Cancer Center, Medical University of South Carolina (National Institutes of Health P30 CA138313) for providing shRNA constructs.

REFERENCES

Abe K, Takeichi M (2008). EPLIN mediates linkage of the cadherin catenin complex to F-actin and stabilizes the circumferential actin belt. Proc Natl Acad Sci USA 105, 13–19.

Ahlenstiel CL, Lim HG, Cooper DA, Ishida T, Kelleher AD, Suzuki K (2012). Direct evidence of nuclear Argonaute distribution during transcriptional silencing links the actin cytoskeleton to nuclear RNAi machinery in human cells. Nucleic Acids Res 40, 1579–1595.

Amano M, Nakayama M, Kaibuchi K (2010). Rho-kinase/ROCK: A key regulator of the cytoskeleton and cell polarity. Cytoskeleton (Hoboken) 67, 545–554.

Anderson CA, Kovar DR, Gardel ML, Winkelman JD (2021). LIM domain proteins in cell mechanobiology. Cytoskeleton (Hoboken) 78, 303–311.

Antoniou A, Baptista M, Carney N, Hanley JG (2014). PICK1 links Argonaute 2 to endosomes in neuronal dendrites and regulates miRNA activity. EMBO Rep 15, 548–556.

Arnold TR, Shawky JH, Stephenson RE, Dinshaw KM, Higashi T, Huq F, Davidson LA, Miller AL (2019). Anillin regulates epithelial cell mechanics by structuring the medial-apical actomyosin network. eLife 8, e39065.

Ashburner M, Ball CA, Blake JA, Botstein D, Butler H, Cherry JM, Davis AP, Dolinski K, Dwight SS, Eppig JT, *et al*. (2000). Gene ontology: tool for the unification of biology. The Gene Ontology Consortium. Nat Genet 25, 25–29.

Bauer K, Kratzer M, Otte M, de Quintana KL, Hagmann J, Arnold GJ, Eckerskorn C, Lottspeich F, Siess W (2000). Human CLP36, a PDZ-domain and LIM-domain protein, binds to alpha-actinin-1 and associates with actin filaments and stress fibers in activated platelets and endothelial cells. Blood 96, 4236–4245.

Beati H, Peek I, Hordowska P, Honemann-Capito M, Glashauser J, Renschler FA, Kakanj P, Ramrath A, Leptin M, Luschnig S, *et al*. (2018). The adherens junction-associated LIM domain protein Smallish regulates epithelial morphogenesis. J Cell Biol 217, 1079–1095.

Bose M, Chatterjee S, Chakrabarty Y, Barman B, Bhattacharyya SN (2020). Retrograde trafficking of Argonaute 2 acts as a rate-limiting step for de novo miRNP formation on endoplasmic reticulum-attached polysomes in mammalian cells. Life Sci Alliance 3, e201800161.

Bridge KS, Shah KM, Li Y, Foxler DE, Wong SCK, Miller DC, Davidson KM, Foster JG, Rose R, Hodgkinson MR, *et al*. (2017). Argonaute utilization for miRNA silencing is determined by phosphorylation-dependent recruitment of LIM-domain-containing proteins. Cell Rep 20, 173–187.

Cavey M, Rauzi M, Lenne PF, Lecuit T (2008). A two-tiered mechanism for stabilization and immobilization of E-cadherin. Nature 453, 751–756.

Chiasson-MacKenzie C, Morris ZS, Baca Q, Morris B, Coker JK, Mirchev R, Jensen AE, Carey T, Stott SL, Golan DE, McClatchey AI (2015). NF2/Merlin mediates contact-dependent inhibition of EGFR mobility and internalization via cortical actomyosin. J Cell Biol 211, 391–405.

Choi W, Acharya BR, Peyret G, Fardin MA, Mege RM, Ladoux B, Yap AS, Fanning AS, Peifer M (2016). Remodeling the zonula adherens in response to tension and the role of afadin in this response. J Cell Biol 213, 243–260.

Coue M, Brenner SL, Spector I, Korn ED (1987). Inhibition of actin polymerization by latrunculin A. FEBS Lett 213, 316–318.

Daulagala AC, Bridges MC, Kourtidis A (2019). E-cadherin beyond structure: A signaling hub in colon homeostasis and disease. Int J Mol Sci 20, 2756.

Daulagala AC, Kourtidis A (2022). ECM Substrates impact RNAi localization at Adherens junctions of colon epithelial cells. Cells 11, 3740.

Denes LT, Kelley CP, Wang ET (2021). Microtubule-based transport is essential to distribute RNA and nascent protein in skeletal muscle. Nat Commun 12, 6079.

Detzer A, Engel C, Wunsche W, Sczakiel G (2011). Cell stress is related to re-localization of Argonaute 2 and to decreased RNA interference in human cells. Nucleic Acids Res 39, 2727–2741.

Farquhar MG, Palade GE (1963). Junctional complexes in various epithelia. J Cell Biol 17, 375–412.

Gagnon KT, Li L, Chu Y, Janowski BA, Corey DR (2014). RNAi factors are present and active in human cell nuclei. Cell Rep 6, 211–221.

Gene Ontology C (2021). The Gene Ontology resource: enriching a GOld mine. Nucleic Acids Res 49, D325–D334.

Golden RJ, Chen B, Li T, Braun J, Manjunath H, Chen X, Wu J, Schmid V, Chang TC, Kopp F, *et al*. (2017). An Argonaute phosphorylation cycle promotes microRNA-mediated silencing. Nature 542, 197–202.

Gomez GA, McLachlan RW, Wu SK, Caldwell BJ, Moussa E, Verma S, Bastiani M, Priya R, Parton RG, Gaus K, *et al*. (2015). An RPTPalpha/Src family kinase/Rap1 signaling module recruits myosin IIB to support contractile tension at apical E-cadherin junctions. Mol Biol Cell 26, 1249–1262.

Gumbiner B, Simons K (1986). A functional assay for proteins involved in establishing an epithelial occluding barrier: identification of a uvomorulin-like polypeptide. J Cell Biol 102, 457–468.

Hammond SM, Boettcher S, Caudy AA, Kobayashi R, Hannon GJ (2001). Argonaute2, a link between genetic and biochemical analyses of RNAi. Science 293, 1146–1150.

Harris TJ, Tepass U (2010). Adherens junctions: from molecules to morphogenesis. Nat Rev Mol Cell Biol 11, 502–514.

Hayward MK, Muncie JM, Weaver VM (2021). Tissue mechanics in stem cell fate, development, and cancer. Dev Cell 56,1833–1847.

Heuze ML, Sankara Narayana GHN, D'Alessandro J, Cellerin V, Dang T, Williams DS, Van Hest JC, Marcq P, Mege RM, Ladoux B (2019). Myosin II isoforms play distinct roles in adherens junction biogenesis. eLife 8, e46599.

Huntzinger E, Izaurralde E (2011). Gene silencing by microRNAs: contributions of translational repression and mRNA decay. Nat Rev Genet 12, 99–110.

Ivanov AI, McCall IC, Parkos CA, Nusrat A (2004). Role for actin filament turnover and a myosin II motor in cytoskeleton-driven disassembly of the epithelial apical junctional complex. Mol Biol Cell 15, 2639–2651.

James V, Zhang Y, Foxler DE, de Moor CH, Kong YW, Webb TM, Self TJ, Feng Y, Lagos D, Chu CY, *et al*. (2010). LIM-domain proteins, LIMD1, Ajuba, and WTIP are required for microRNA-mediated gene silencing. Proc Natl Acad Sci USA 107, 12499–12504.

Janmey PA, Fletcher DA, Reinhart-King CA (2020). Stiffness sensing by cells. Physiol Rev 100, 695–724.

Kadrmas JL, Beckerle MC (2004). The LIM domain: from the cytoskeleton to the nucleus. Nat Rev Mol Cell Biol 5, 920–931.

Kanai Y, Dohmae N, Hirokawa N (2004). Kinesin transports RNA: isolation and characterization of an RNA-transporting granule. Neuron 43, 513–525.

Kourtidis A, Anastasiadis PZ (2016). PLEKHA7 defines an apical junctional complex with cytoskeletal associations and miRNA-mediated growth implications. Cell Cycle 15, 498–505.

Kourtidis A, Lu R, Pence LJ, Anastasiadis PZ (2017a). A central role for cadherin signaling in cancer. Exp Cell Res 358, 78–85.

Kourtidis A, Necela B, Lin WH, Lu R, Feathers RW, Asmann YW, Thompson EA, Anastasiadis PZ (2017b). Cadherin complexes recruit mRNAs and RISC to regulate epithelial cell signaling. J Cell Biol 216, 3073–3085.

Kourtidis A, Dighera B, Risner A, Hackemack R, Nikolaidis N (2022). Origin and evolution of the multifaceted Adherens junction component Plekha7. Front Cell Dev Biol 10, 856975.

Kovacs EM, Goodwin M, Ali RG, Paterson AD, Yap AS (2002). Cadherin-directed actin assembly: E-cadherin physically associates with the Arp2/3 complex to direct actin assembly in nascent adhesive contacts. Curr Biol 12, 379–382.

Kovacs M, Toth J, Hetenyi C, Malnasi-Csizmadia A, Sellers JR (2004). Mechanism of blebbistatin inhibition of myosin II. J Biol Chem 279, 35557–35563.

Kovacs EM, Verma S, Ali RG, Ratheesh A, Hamilton NA, Akhmanova A, Yap AS (2011). N-WASP regulates the epithelial junctional actin cytoskeleton through a non-canonical post-nucleation pathway. Nat Cell Biol 13, 934–943.

Leerberg JM, Gomez GA, Verma S, Moussa EJ, Wu SK, Priya R, Hoffman BD, Grashoff C, Schwartz MA, Yap AS (2014). Tension-sensitive actin assembly supports contractility at the epithelial zonula adherens. Curr Biol 24, 1689–1699.

Leung AK, Calabrese JM, Sharp PA (2006). Quantitative analysis of Argonaute protein reveals microRNA-dependent localization to stress granules. Proc Natl Acad Sci USA 103, 18125–18130.

Levayer R, Lecuit T (2012). Biomechanical regulation of contractility: spatial control and dynamics. Trends Cell Biol 22, 61–81.

Liao YC, Fernandopulle MS, Wang G, Choi H, Hao L, Drerup CM, Patel R, Qamar S, Nixon-Abell J, Shen Y, *et al*. (2019). RNA Granules hitchhike on lysosomes for long-distance transport, using Annexin A11 as a molecular tether. Cell 179, 147–164 e120.

Lin YH, Zhen YY, Chien KY, Lee IC, Lin WC, Chen MY, Pai LM (2017). LIMCH1 regulates nonmuscle myosin-II activity and suppresses cell migration. Mol Biol Cell 28, 1054–1065.
Lindsay AJ, McCaffrey MW (2011). Myosin Va is required for P body but not stress granule formation. J Biol Chem 286, 11519–11528.
Liu J, Carmell MA, Rivas FV, Marsden CG, Thomson JM, Song JJ, Hammond SM, Joshua-Tor L, Hannon GJ (2004). Argonaute2 is the catalytic engine of mammalian RNAi. Science 305, 1437–1441.
Maeda M, Asano E, Ito D, Ito S, Hasegawa Y, Hamaguchi M, Senga T (2009). Characterization of interaction between CLP36 and palladin. FEBS J 276, 2775–2785.
Matsuda M, Chu CW, Sokol SY (2022). Lmo7 recruits myosin II heavy chain to regulate actomyosin contractility and apical domain size in Xenopus ectoderm. Development 149, dev200236.
McCaffrey MW, Lindsay AJ (2012). Roles for myosin Va in RNA transport and turnover. Biochem Soc Trans 40, 1416–1420.
Mege RM, Ishiyama N (2017). Integration of Cadherin adhesion and cytoskeleton at Adherens junctions. Cold Spring Harb Perspect Biol 9, a028738.
Meister G, Landthaler M, Patkaniowska A, Dorsett Y, Teng G, Tuschl T (2004). Human Argonaute2 mediates RNA cleavage targeted by miRNAs and siRNAs. Mol Cell 15, 185–197.
Mendonsa AM, Na TY, Gumbiner BM (2018). E-cadherin in contact inhibition and cancer. Oncogene 37, 4769–4780.
Meng W, Mushika Y, Ichii T, Takeichi M (2008). Anchorage of microtubule minus ends to adherens junctions regulates epithelial cell-cell contacts. Cell 135, 948–959.
Meng W, Takeichi M (2009). Adherens junction: molecular architecture and regulation. Cold Spring Harb Perspect Biol 1, a002899.
Mi H, Muruganujan A, Ebert D, Huang X, Thomas PD (2019). PANTHER version 14: more genomes, a new PANTHER GO-slim and improvements in enrichment analysis tools. Nucleic Acids Res 47, D419–D426.
Moro A, Driscoll TP, Boraas LC, Armero W, Kasper DM, Baeyens N, Jouy C, Mallikarjun V, Swift J, Ahn SJ, *et al.* (2019). MicroRNA-dependent regulation of biomechanical genes establishes tissue stiffness homeostasis. Nat Cell Biol 21, 348–358.
Nair-Menon J, Daulagala AC, Connor DM, Rutledge L, Penix T, Bridges MC, Wellslager B, Spyropoulos DD, Timmers CD, Broome AM, Kourtidis A (2020). Predominant distribution of the RNAi machinery at apical Adherens junctions in colonic epithelia is disrupted in cancer. Int J Mol Sci 21, 2559.
Ooshio T, Irie K, Morimoto K, Fukuhara A, Imai T, Takai Y (2004). Involvement of LMO7 in the association of two cell-cell adhesion molecules, nectin and E-cadherin, through afadin and alpha-actinin in epithelial cells. J Biol Chem 279, 31365–31373.
Pichon X, Moissoglu K, Coleno E, Wang T, Imbert A, Robert MC, Peter M, Chouaib R, Walter T, Mueller F, *et al.* (2021). The kinesin KIF1C transports APC-dependent mRNAs to cell protrusions. RNA 27, 1528–1544.
Priya R, Yap AS, Gomez GA (2013). E-cadherin supports steady-state Rho signaling at the epithelial zonula adherens. Differentiation 86, 133–140.
Pulimeno P, Bauer C, Stutz J, Citi S (2010). PLEKHA7 is an adherens junction protein with a tissue distribution and subcellular localization distinct from ZO-1 and E-cadherin. PLoS One 5, e12207.
Ramirez Moreno M, Bulgakova NA (2021). The Cross-talk between EGFR and E-Cadherin. Front Cell Dev Biol 9, 828673.
Ran FA, Hsu PD, Wright J, Agarwala V, Scott DA, Zhang F (2013). Genome engineering using the CRISPR-Cas9 system. Nat Protoc 8, 2281–2308.
Ratheesh A, Yap AS (2012). A bigger picture: classical cadherins and the dynamic actin cytoskeleton. Nat Rev Mol Cell Biol 13, 673–679.
Reynolds AB, Daniel J, McCrea PD, Wheelock MJ, Wu J, Zhang Z (1994). Identification of a new catenin: the tyrosine kinase substrate p120cas associates with E-cadherin complexes. Mol Cell Biol 14, 8333–8342.
Rouaud F, Huang W, Flinois A, Jain K, Vasileva E, Di Mattia T, Mauperin M, Parry DAD, Dugina V, Chaponnier C, *et al.* (2023). Cingulin and paracingulin tether myosins-2 to junctions to mechanoregulate the plasma membrane. J Cell Biol 222.
Salvi AM, DeMali KA (2018). Mechanisms linking mechanotransduction and cell metabolism. Curr Opin Cell Biol 54, 114–120.
Scarborough EA, Uchida K, Vogel M, Erlitzki N, Iyer M, Phyo SA, Bogush A, Kehat I, Prosser BL (2021). Microtubules orchestrate local translation to enable cardiac growth. Nat Commun 12, 1547.
Schindelin J, Arganda-Carreras I, Frise E, Kaynig V, Longair M, Pietzsch T, Preibisch S, Rueden C, Saalfeld S, Schmid B, *et al.* (2012). Fiji: an open-source platform for biological-image analysis. Nat Methods 9, 676–682.
Shewan AM, Maddugoda M, Kraemer A, Stehbens SJ, Verma S, Kovacs EM, Yap AS (2005). Myosin 2 is a key Rho kinase target necessary for the local concentration of E-cadherin at cell-cell contacts. Mol Biol Cell 16, 4531–4542.
Skare P, Kreivi JP, Bergstrom A, Karlsson R (2003). Profilin I colocalizes with speckles and Cajal bodies: a possible role in pre-mRNA splicing. Exp Cell Res 286, 12–21.
Smutny M, Cox HL, Leerberg JM, Kovacs EM, Conti MA, Ferguson C, Hamilton NA, Parton RG, Adelstein RS, Yap AS (2010). Myosin II isoforms identify distinct functional modules that support integrity of the epithelial zonula adherens. Nat Cell Biol 12, 696–702.
Sumi A, Hayes P, D'Angelo A, Colombelli J, Salbreux G, Dierkes K, Solon J (2018). Adherens junction length during tissue contraction is controlled by the mechanosensitive activity of actomyosin and junctional recycling. Dev Cell 47, 453–463 e453.
Takeichi M (1995). Morphogenetic roles of classic cadherins. Curr Opin Cell Biol 7, 619–627.
Takeichi M (2014). Dynamic contacts: rearranging adherens junctions to drive epithelial remodelling. Nat Rev Mol Cell Biol 15, 397–410.
Tamura N, Ohno K, Katayama T, Kanayama N, Sato K (2007). The PDZ-LIM protein CLP36 is required for actin stress fiber formation and focal adhesion assembly in BeWo cells. Biochem Biophys Res Commun 364, 589–594.
Tang VW, Brieher WM (2012). alpha-Actinin-4/FSGS1 is required for Arp2/3-dependent actin assembly at the adherens junction. J Cell Biol 196, 115–130.
Thoreson MA, Anastasiadis PZ, Daniel JM, Ireton RC, Wheelock MJ, Johnson KR, Hummingbird DK, Reynolds AB (2000). Selective uncoupling of p120(ctn) from E-cadherin disrupts strong adhesion. J Cell Biol 148, 189–202.
Tilley AMC, Howard CM, Sridharan S, Subramaniyan B, Bearss NR, Alkhalili S, Raman D (2020). The CXCR4-dependent LASP1-Ago2 interaction in triple-negative breast cancer. Cancers (Basel) 12, 2455.
Uyeda TQ, Iwadate Y, Umeki N, Nagasaki A, Yumura S (2011). Stretching actin filaments within cells enhances their affinity for the myosin II motor domain. PLoS One 6, e26200.
Vallenius T, Luukko K, Makela TP (2000). CLP-36 PDZ-LIM protein associates with nonmuscle alpha-actinin-1 and alpha-actinin-4. J Biol Chem 275, 11100–11105.
Verma S, Han SP, Michael M, Gomez GA, Yang Z, Teasdale RD, Ratheesh A, Kovacs EM, Ali RG, Yap AS (2012). A WAVE2-Arp2/3 actin nucleator apparatus supports junctional tension at the epithelial zonula adherens. Mol Biol Cell 23, 4601–4610.
Vicente-Manzanares M, Ma X, Adelstein RS, Horwitz AR (2009). Non-muscle myosin II takes centre stage in cell adhesion and migration. Nat Rev Mol Cell Biol 10, 778–790.
Wayt J, Cartagena-Rivera A, Dutta D, Donaldson JG, Waterman CM (2021). Myosin II isoforms promote internalization of spatially distinct clathrin-independent endocytosis cargoes through modulation of cortical tension downstream of ROCK2. Mol Biol Cell 32, 226–236.
Yamada A, Irie K, Fukuhara A, Ooshio T, Takai Y (2004). Requirement of the actin cytoskeleton for the association of nectins with other cell adhesion molecules at adherens and tight junctions in MDCK cells. Genes Cells 9, 843–855.
Yamada S, Nelson WJ (2007). Localized zones of Rho and Rac activities drive initiation and expansion of epithelial cell-cell adhesion. J Cell Biol 178, 517–527.
Yamamoto K, Miura H, Ishida M, Mii Y, Kinoshita N, Takada S, Ueno N, Sawai S, Kondo Y, Aoki K (2021). Optogenetic relaxation of actomyosin contractility uncovers mechanistic roles of cortical tension during cytokinesis. Nat Commun 12, 7145.
Yonemura S, Wada Y, Watanabe T, Nagafuchi A, Shibata M (2010). alpha-Catenin as a tension transducer that induces adherens junction development. Nat Cell Biol 12, 533–542.
Yu Y, Elble RC (2016). Homeostatic Signaling by Cell-Cell Junctions and Its Dysregulation during Cancer Progression. J Clin Med 5, E26.
Yu-Kemp HC, Szymanski RA, Cortes DB, Gadda NC, Lillich ML, Maddox AS, Peifer M (2022). Micron-scale supramolecular myosin arrays help mediate cytoskeletal assembly at mature adherens junctions. J Cell Biol 221, e202103074.
Yulis M, Kusters DHM, Nusrat A (2018). Cadherins: cellular adhesive molecules serving as signalling mediators. J Physiol 596, 3883–3898.
Zeng Y, Sankala H, Zhang X, Graves PR (2008). Phosphorylation of Argonaute 2 at serine-387 facilitates its localization to processing bodies. Biochem J 413, 429–436.